Thermokarst processes increase the supply of stabilizing surfaces and elements (Fe, Mn, Al, Ca) for mineral-organic carbon interactions

Arthur Monhonval[1*], Jens Strauss[2], Maxime Thomas[1], Catherine Hirst[1], Hugues Titeux[1], Justin Louis[1], Alexia Gilliot[1], Eléonore du Bois d'Aische[1], Benoît Pereira[1], Aubry Vandeuren[1], Guido Grosse[2,3], Lutz Schirrmeister[2], Loeka L. Jongejans[2,3], Mathias Ulrich[4], Sophie Opfergelt[1]

[1]Earth and Life Institute, Université catholique de Louvain, Louvain-la-Neuve, Belgium
[2]Permafrost Research Section, Alfred Wegener Institute Helmholtz Centre for Polar and Marine Research, Potsdam, Germany
[3]Institute of Geosciences, University of Potsdam, Potsdam, Germany
[4]Institute for Geography, Leipzig University, Leipzig, Germany[1]

*Correspondence: Arthur Monhonval (arthur.monhonval@uclouvain.be)
https://orcid.org/0000-0003-0038-182X

Jens Strauss (jens.strauss@awi.de) - https://orcid.org/0000-0003-4678-4982
Maxime Thomas (maxime.thomas@uclouvain.be) -
Catherine Hirst (catherine.hirst@uclouvain.be)
Hugues Titeux (hugues.titeux@uclouvain.be)
Justin Louis (justin.louis@student.uclouvain.be)
Alexia Gilliot (alexia.gilliot@student.uclouvain.be)
Eléonore du Bois d'Aische (eleonore.dubois@student.uclouvain.be)
Benoît Pereira (benoit.pereira@uclouvain.be)
Aubry Vandeuren (aubry.vandeuren@uclouvain.be)
Guido Grosse (guido.grosse@awi.de) - https://orcid.org/0000-0001-5895-2141
Lutz Schirrmeister (lutz.schirrmeister@awi.de) - https://orcid.org/0000-0001-9455-0596
Loeka L. Jongejans (loeka.jongejans@awi.de) - https://orcid.org/0000-0002-0383-4567
Mathias Ulrich (mathias.ulrich@uba.de) - https://orcid.org/0000-0002-1337-252X
Sophie Opfergelt (sophie.opfergelt@uclouvain.be) - https://orcid.org/0000-0002-1773-4823

Keywords: permafrost, Yedoma, thaw, redox processes, organic carbon stabilization, Arctic

Abstract

The stabilizing properties of mineral-organic carbon interactions have been studied in many soil environments (temperate soils, podzol lateritic soils, paddy soils). Recently, interest in their role in permafrost regions is increasing as permafrost was identified as a hotspot of change. In thawing ice-rich permafrost regions, such as the Yedoma domain, 327-466 Gt of frozen organic carbon (OC) is buried in deep sediments. Interactions between minerals and OC are important since the OC is located in close contact with the mineral matrix. Mineral surfaces and elements could mitigate recent and future greenhouse gas emissions through physical and/or physico-chemical protection of OC. The dynamic changes of redox and pH conditions associated with thermokarst lake formation and drainage, trigger metal-oxide dissolution and precipitation, likely influencing OC stabilization and microbial mineralization. However, the influence of thermokarst processes on mineral-OC interactions remains poorly constrained. In this study, we aim to characterize Fe, Mn, Al and Ca minerals and their potential protective role for OC. Total and selective extractions were used to assess the crystalline and amorphous oxides or complexed metal pools as well as the organic acids found within these pools. We analyzed four sediment cores from an ice-rich permafrost area in Central Yakutia, which were drilled i) in

[1] M. Ulrich present address: German Federal Environment Agency, Dessau-Roßlau, Germany

undisturbed Yedoma uplands, ii) beneath a recent lake formed within Yedoma deposits, iii) in a drained thermokarst lake basin, and iv) beneath a mature thermokarst lake from the early Holocene period. We find a decrease in the amount of reactive Fe, Mn, Al and Ca in the deposits upon lake formation (promoting reduction reactions), and this was largely balanced by an increase in the amount of reactive metals in the deposits upon lake drainage (promoting oxidation reactions). We demonstrate an increase in the metal:C molar ratio upon thermokarst process, which may indicate an increase of metal-C bindings and could provide a higher protective role against microbial mineralization of organic matter. Finally, we find that an increase in mineral-OC interactions corresponded to a decrease in CO_2 and CH_4 gas emissions upon thermokarst process. Mineral-OC interactions could mitigate greenhouse gas production from permafrost thaw as soon as lake drainage occurs.

Acknowledgements

This project received funding from the European Union's Horizon 2020 research and innovation program under grant agreement No. 714617 to SO, and SO acknowledges funding from the Fund for Scientific Research FNRS in Belgium (FC69480). Field sample collection was funded by a European Research Council (ERC) Starting Grant Peta-Carb to GG as well as Alfred Wegener Institute basic funding. The authors acknowledge the Mineral and Organic Chemical Analysis (MOCA) platform at UCLouvain for conducting chemical analysis. The authors would like to thank Elisabeth Mauclet, Yannick Agnan and Pierre Delmelle for fruitful discussions. We thank the associate editor and the two reviewers for their constructive comments.

1 Introduction

Permafrost deposits are thawing at an unprecedented rate since the last century (Koven et al., 2011; Schuur et al., 2015; Biskaborn et al., 2019). Climatic warming, which is two to three times more intense in northern regions, will accentuate permafrost thaw in coming decades affecting the whole Arctic (IPCC, 2021). Thereby, the organic carbon (OC) stored in the permafrost deposits is mobilized. Even if a portion of the 1,300 Pg OC stock lying within permafrost regions (Hugelius et al., 2014; Strauss et al., 2017) is decomposed upon thawing, this would result in significant greenhouse gas emissions at the global scale (IPCC, 2021). Thawing of Yedoma (i.e., ice-rich permafrost) deposits leads to massive landscape modifications (Grosse et al., 2013; Schirrmeister et al., 2013; Strauss et al., 2021). The melting of ice-wedge networks and other excess ice usually leads to surface subsidence followed by thermokarst lake formation. With time, the lake can extend horizontally and vertically, and eventually create a drainage pathway (Grosse et al., 2013). Upon lake drainage, sediment deposits remain within the dried basins, which are called "Alas". At the Arctic scale, lake and drained lake basin systems can represent up to ~50% of the circumpolar Northern Hemisphere permafrost region lowland areas (Jones et al., 2022). About a quarter of 21st century thermokarst lake CH_4 release stems from newly thawed OC stored in deep deposits from the Yedoma region (Schneider von Deimling et al., 2015). The thawing and draining of ice-rich deposits triggers shifts in soil or sediment properties, such as the reductive-oxidative potential (i.e., redox) or pH values. These shifts drive changes in biogeochemical processes with potential consequences for mineral-OC interactions (i.e., aggregation, organo-mineral associations, organo-metallic complexes; Kleber et al., 2015) and thus OC mineralization rates (von Lützow et al., 2006; Jones et al., 2022). These processes, leading to destabilization of these mineral-OC interactions, may accelerate permafrost carbon emissions, and need to be incorporated in earth system models for more comprehensive projections of the permafrost carbon feedback (Schuur et al., 2015; Opfergelt, 2020).

Mineral elements and mineral surfaces provide stabilizing mechanisms for OC resulting in the mitigation of OC mineralization in many soils (Torn et al., 1997; Dutta et al., 2006; von Lützow et al., 2006; Mikutta et al., 2007; Kögel-Knabner et al., 2008; Wagai et al., 2013; Gentsch et al., 2015b; Kleber et al., 2015; Kramer and Chadwick, 2018; Hemingway et al., 2019). Organic carbon stabilizing mechanisms involving Fe and Al oxy(hydr)oxide have been extensively studied in i) controlled

conditions (Schwertmann, 1991; Eusterhues et al., 2008; Huang and Hall, 2017; Zhao et al., 2017), ii) agricultural soils (Wang et al., 2019), iii) tropical lateritic soils (Fritsch et al., 2009; Mikutta et al., 2009; Inagaki et al., 2020), iv) peatlands and rice paddy soils (Fiedler and Sommer, 2004; Kögel-Knabner et al., 2010; Pan et al., 2014; Xue et al., 2019), and v) lake and marine sediments (Eglinton, 2012; Lalonde et al., 2012; Barber et al., 2017). However, more recently there has been an increasing interest in permafrost regions (Fiedler et al., 2004; Mu et al., 2016; Herndon et al., 2017, 2020; Patzner et al., 2020; Sowers et al., 2020; Monhonval et al., 2021b; Joss et al., 2022; Lim et al., 2022b). In addition, Mn and Ca play a key role in OC stabilization and degradation mechanisms (Bartlett and Ross, 2005; Johnson et al., 2015; Oldham et al., 2017; Rowley et al., 2018; Sowers et al., 2020; Li et al., 2021). Together Fe, Al, Mn and Ca –bearing minerals and cations can provide physical and physico-chemical protection of OC. For microbial mineralization, OC has to be in intimate contact with microorganisms. Physical protection of OC within mineral aggregates prevents microorganisms from approaching this substrate and thus limits this contact. Physico-chemical protection, in the form of organo-mineral associations within clays or Fe-, Mn-, Al-(oxyhydr)oxides using polyvalent cation bridges such as Fe^{3+}, Al^{3+}, Ca^{2+}, Mn^{3+} (adsorption) or in the form of organo-metallic complexes (Fe-, Mn-, Al- and Ca-OC; complexation), hinders microbial degradation through diverse type of chemical bindings (e.g., Lutzow et al., 2006). Overall, physical and physico-chemical protection of OC through mineral-OC interactions lower the solubility of organic acids and their availability for microorganisms.

A major concern is that mineral-OC interactions that promote OC stabilization could be highly reversible under changing physico-chemical conditions, including both redox and pH (von Lützow et al., 2006; Schmidt et al., 2011; Grant et al., 2022) that occur during thermokarst processes. Fluctuating wet-dry cycles drive redox shifts in otherwise well-drained soils resulting in mineral dissolution, OC mobilization, and subsequent OC mineralization (Bartlett and Ross, 2005; Lipson et al., 2012; Ernakovich et al., 2017; Possinger et al., 2020; Kappler et al., 2021; Kleber et al., 2021). These shifts in redox potential influence redox-sensitive elements (i.e., Fe and Mn) by modifying the crystallinity of Fe- and Mn-oxy(hydr)oxides or the redistribution of stabilizing surfaces, with subsequent OC release (Winkler et al., 2018; Inagaki et al., 2020; Patzner et al., 2020; Monhonval et al., 2021b). The processes of wetting and drying are also evident in thawed lake basins. The reductive conditions induced upon lake formation may have an opposite influence on mineral-OC interactions compared to the oxidative potential induced upon lake drainage. Along the redox ladder (Figure 1), electron acceptors follow the sequence O_2, NO_3^-, NO_2^-, Mn^{4+}, Fe^{3+}, SO_4^-, CO_2, from more to less thermodynamically efficient. However, studies show that these redox reactions often overlap under environmental conditions (e.g., Kappler et al., 2021). Besides the redox conditions, the pH is also a key driver of Al-, Fe-, Mn-oxy(hydr)oxide solubility and dissolution rates (Kleber et al., 2015). Furthermore, in soils/sediments with a high pH (neutral/alkaline), Ca promotes OC stabilization via aggregation, cation bridging and/or complexation (von Lützow et al., 2006; Rowley et al., 2018; Wang et al., 2021) and may also raise the surface potential of Fe-, Mn-, Al-oxy-(hydr)oxides which lead to more effective coagulation of OC (Davis and Edwards, 2017). The contribution of Ca towards OC stabilization was even described in permafrost systems (Sowers et al., 2020). In soils with an acidic/neutral pH, the loss of Ca-based stabilizing mechanisms enables OC microbial degradation (Rowley et al., 2018).

Most mineral-OC interactions studies focus on one or a few elements involved in OC stabilization but, to our knowledge, very few investigated Fe, Mn, Al and Ca interactions with OC simultaneously. In ice-rich permafrost regions, interactions between minerals and OC are crucial given that most of the OC is found in deep mineral sediments, potentially enhancing interactions between the mineral and the organic compounds upon thaw (Hemingway et al., 2019; Lim et al., 2022b, 2022a). Although the increase of Fe stabilizing surfaces from undisturbed (not thawed since deposition) Yedoma deposits to previously thawed Alas deposits was recently shown (Monhonval et al., 2021b), neither the influence of thermokarst lake formation and drainage on mineral-OC interactions in sediments, nor the role of all potential reactive metals (Fe, Mn, Al and Ca) were investigated. We hypothesize that lake formation

and lake drainage are important intermediate steps controlling changes in mineral-OC interactions upon thermokarst process, with likely opposing effects.

To test our hypothesis, we studied a landscape transect in Central Yakutia from undisturbed sediments in Yedoma uplands to drained lake sediments and sediments below thermokarst lakes from different generations (Ulrich et al., 2017). The different thawing history of these deposits allows us to dissociate thermokarst lake formation on the one hand and thermokarst lake drainage and refreezing on the other hand. This comparison provides a glance into the evolution of ice-rich permafrost deposits in the near future, and allows us to assess how mineral-OC interactions (with Fe, Mn, Al and Ca) will evolve within the thawed, drained and refrozen deposits.

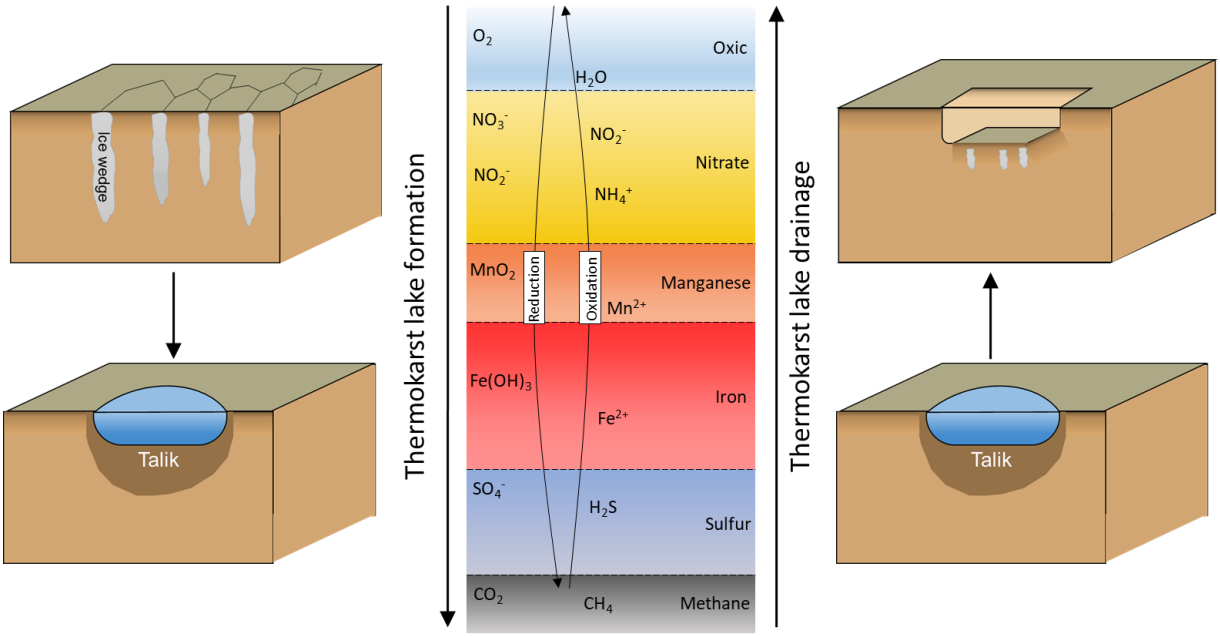

Figure 1. Simplified view of the oxidation/reduction couples involved in redox reactions and listed in thermodynamic order. The redox potential is decreasing towards the bottom of the column. Upon thermokarst lake formation (left), electron acceptors for reactions follow the sequence O_2, NO_3^-, MnO_2, Fe^{3+}, SO_4^- and CO_2. Upon lake drainage (right), the redox potential increases and favors oxidation reactions. The coloured panels indicate the sequence in which the different reactions are expected to occur on the basis of thermodynamics; however, these redox reactions may overlap under environmental conditions (modified from Melton et al., (2014)).

2 Regional settings

The studied Yukechi site is located 80 km southeast from the city of Yakutsk in the central part of the Sakha (Yakut) Republic, East Siberia, Russia (Figure 2a). The region is characterized by a cold and continental climate with a mean annual temperature of -10.7°C (mean January: -41°C, mean July: 18.5°C) and a mean annual precipitation of 246 mm (period: 1982–2012; Yakutsk Weather Station: RSM00024959; Climate-data.org, 2022). Between 1966 and 2016, the Central Yakutian mean annual air temperature has increased by 0.3-0.6°C per decade (Gorokhov and Fedorov, 2018). Central Yakutia lies within the continuous permafrost zone and is in a low-relief landscape, characterized by numerous Alas basins and thermokarst lakes at different evolutionary stages (Soloviev, 1959; Tarasenko, 2013), indicating past and modern active thermokarst processes (Ulrich et al., 2017).

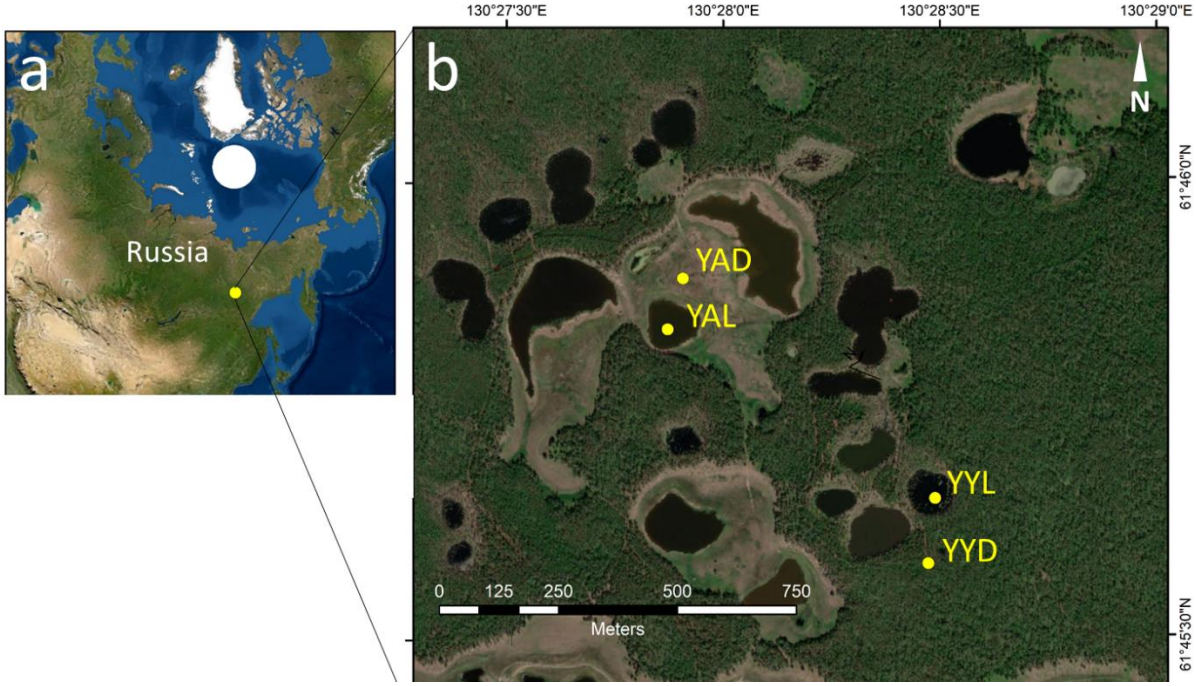

Figure 2. (a) Location of the Yukechi site in Russia. (b) Location of the four cores within Yukechi site: the Yedoma dry (YYD), the Yedoma lake (YYL), the Alas dry (YAD) and the Alas lake core (YAL). Source: Esri, DigitalGlobe, GeoEye, Earthstar Geographics, CNES/Airbus DS, USDA, USGS, AeroGRID, IGN, and the GIS User Community.

The Yukechi site is located within the Yedoma domain (Strauss et al., 2021). The Yedoma deposits of this region can be more than 30 m thick (Soloviev, 1959). For tens of millennia, cold and dry conditions during late Pleistocene and continuous sedimentation led to the accumulation of several tens of meters thick Yedoma deposits with characteristic ice-wedge formation (I) (Figure 3a). These ice-wedges formed by the infilling of vertical frost cracks with snow melt water repeatedly (Schirrmeister et al., 2013). Warm and wet climate conditions during the Holocene period led to ice wedge melting and a thermokarst lake formed within the subsidence area (II). With time, evaporation and thermokarst lake expansion in depth (i.e., talik deepening) or laterally (i.e., thermoerosion) led to the drainage of the thermokarst basin, and consequent refreezing of the deposits (III) (Grosse et al., 2013). Since the onset of the Holocene until now, lake formation and potential drainage have occurred within the refrozen Alas basin or within frozen Yedoma deposits (IV).

The studied transect included four evolutionary stages: undisturbed Yedoma sediments (Yedoma dry), sediments underneath a recently formed lake (Yedoma lake), Alas sediments in a drained thermokarst lake basin (Alas dry), and sediments underneath a lake in the drained basin which have been subject to multiple lake generations (Alas lake) (Figure 2b and Figure 3b). The Yedoma lake is a recent lake that formed in Yedoma uplands about 70 years ago (Yedoma lake), defined here as initial lake formation (lake formation timeline observed by aerial photography from 1944 until today; Ulrich et al., 2017). This recent thermokarst lake formation in the Yedoma uplands indicates still ongoing thermokarst processes (Ulrich et al., 2017, 2021). The Alas sediments experienced drainage/evaporation and refreezing in previous thermokarst lake generations (Jongejans et al., 2021b). In the following, we will split the thermokarst process using specific stages: i) thawing and initial lake formation (*), ii) lake drainage and refreezing (**), and iii) secondary thawing and mature lake formation (***) (Figure 3c). Yedoma and Alas deposits can be clearly subdivided in different stratigraphic units which reflect varying sedimentation processes confirmed by grain-size analysis, as described for the Yedoma dry and Alas dry cores (Windirsch et al., 2020) and for the Yedoma and Alas core beneath the lakes (Jongejans et al., 2021b; Ulrich et al., 2021).

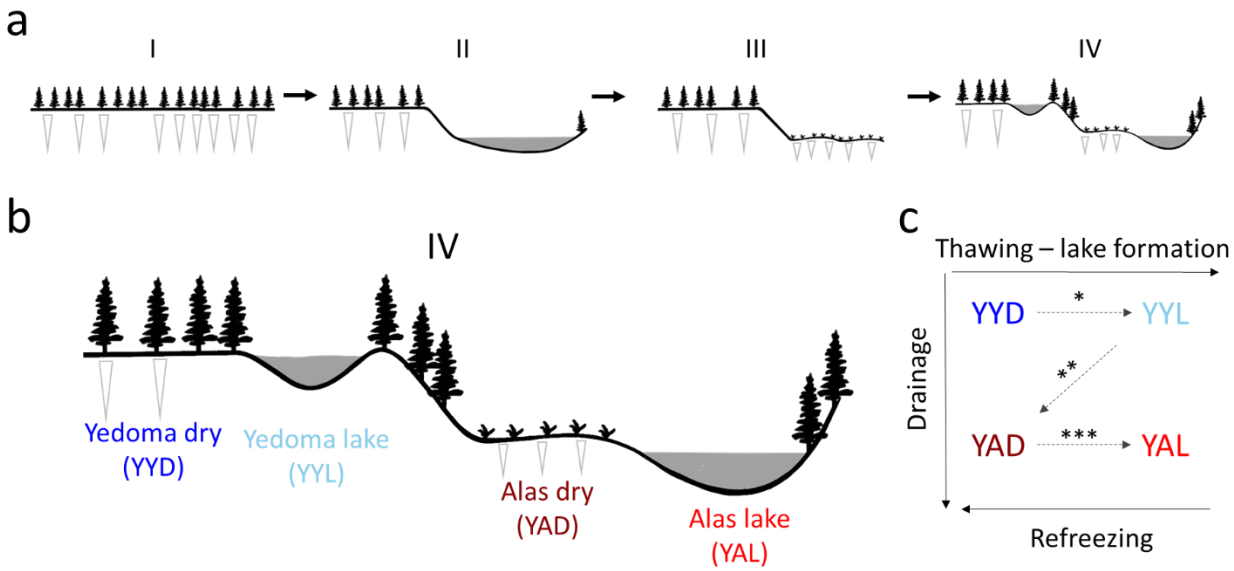

Figure 3. (a) Scheme of the permafrost degradation history (I-IV) of the site sampled in this study. Previous Yedoma uplands, with characteristic ice-wedges (white triangles), have experienced thermokarst process with thermokarst basin formation and drainage since the onset of the Holocene until now (I-III). More recently, about 70 years ago, a thermokarst lake formed in the Yedoma uplands (IV). (b) Sediment cores retrieved from the Yukechi site include a core from the Yedoma uplands (Yukechi Yedoma dry (YYD)), a core beneath a recent Yedoma lake (Yukechi Yedoma lake (YYL)), a core from a drained thermokarst lake basin (Yukechi Alas dry (YAD)), and a core beneath a mature Alas lake (Yukechi Alas lake (YAL)). (c) Permafrost degradation processes involved within each core: *thawing and initial lake formation, **drainage and refreezing, and *** secondary thawing and mature lake formation. The combination of initial lake formation (*) and drainage and refreezing (**) will be referred as the shift from Yedoma dry to Alas dry cores.

3 Materials and Methods

3.1 Coring and sample preparation

The field campaign to Yukechi was carried out in March 2015 to retrieve four sediment cores from different landforms features (Sect. 2): a Yedoma dry core (YYD), a Yedoma lake core (YYL), an Alas dry core (YAD), and an Alas lake core (YYL) (coordinates in Supplementary Table S1). Drilling was carried out using a URB2-4T drilling rig mounted on a truck. The cores were drilled with 15.7 cm diameter for the uppermost parts and 8 cm in diameter in the lower parts. The sediment cores were removed from the core barrel using compressed air, described, stored in plastic bags and kept frozen until laboratory analysis. The drilling depths below surface (i.e. lake-ice surface for lake cores) were 22.4 m (YYD), 17.2 m (YYL), 19.8 m (YAD) and 17.7 m (YAL), respectively (Supplementary Figure S1). Upon coring, the presence of taliks, i.e., portion of the sediments that remain unfrozen during winter, sometimes led to partial core loss (Jongejans et al., 2021b; Ulrich et al., 2021). The Yedoma dry core included an ice wedge between 700 to 950 cm b.s. (below surface) and a talik section was identified between 100 and 200 cm b.s. The Yedoma lake core was frozen below 12 m with significant core loss upon core retrieval for the upper unfrozen section. In the Alas dry core, a talik was found between 160 down to 750 cm b.s. The Alas lake core was unfrozen for the entire core. The frozen cores were split lengthwise using a band saw and were subsequently subsampled in a freezer room at −5°C (sample positions along the core are shown in Supplementary Figure S1). Samples were then air-dried before analyses. In total, 39 samples were analyzed in this study. The locations and numbers of samples analyzed are indicated in Supplementary Table S1.

3.2 Sample characterization

3.2.1 pH and mineralogy

Sample pH-H_2O and pH-KCl (1M KCl solution) were measured on bulk sediment samples (n = 39) with a 1:5 sediment:solution ratio (Page et al., 1982). The pH was measured using WTW Inlolab 720 pH-meter probe after 1 hour with manual shaking every 20 minutes. Bulk sediment mineralogy was determined by X-ray diffraction (XRD; n = 39). The mineralogy of bulk samples was determined on finely ground powder (Cu Kα, Bruker D8 Advance diffractometer, detection limit = 5%). Diffraction spectra were analyzed with DiffracPlus EVA© software version 10.0.0.3 and the PDF-2 (International Centre for Diffraction Data, 2013) and EVA©-embedded DiffracPlus Reference databases (Mineral and Master datasets) using peak fitting method.

3.2.2 Total Fe, Mn, Al and Ca concentrations measurement

Total mineral element concentrations (Fe, Mn, Al and Ca) were measured (n = 39) using a portable X-ray fluorescence (pXRF) device and corrected with inductively-coupled plasma optical emission spectrometry (ICP-OES) measurement after alkaline fusion. This procedure is fully described in Monhonval et al. (2021a). This procedure consists in converting raw pXRF element concentrations values by a linear regression model in order to be equivalent to an ICP-OES concentration value obtained after alkaline fusion. Here, only pXRF concentration values corrected using element specific regressions with high coefficient of determination ($R^2 > 0.72$) were used.

We performed the pXRF measurements in the laboratory on dried samples to avoid variability of water content upon measurements (n = 39) (Ravansari et al., 2020). For this, air or freeze-dried samples are placed in a circular plastic cap (2.5 cm diameter) provided at its base with a transparent thin film (prolene 4 µm). Measurements were carried out using pXRF device Niton XL3t GOLDD+ (Thermo Fisher Scientific) and a lead stand to protect the operator from X-rays. Total time of measurements were set to 90 s (Monhonval et al., 2021a).

For the alkaline fusion used to calibrate the linear regression, air- or freeze-dried samples were ground in an agate mill. A portion (80 mg) of the milled sample was mixed with Li-metaborate and Li-tetraborate and heated during 10 minutes in a 1,000°C oven. The fusion bead was dissolved in HNO_3 2.2N at 80°C and stirred until complete dissolution. We measured mineral element concentrations in that solution by ICP-OES (iCAP 6500 Thermo Fisher Scientific). Loss on ignition was measured to evaluate the sum of oxides (between 98 and 102%) and the concentration values were reported in reference to the sediment dry weight (105°C). The ICP-OES method was performed on a subset of Yukechi samples (n = 6) to confirm that the linear regression from the Yedoma domain (n = 144) (Monhonval et al., 2021a) was appropriate for Yukechi samples (Supplementary Figure S2).

3.2.3 Selective Fe, Mn, Al, Ca and organic carbon extraction methods

Commonly-used selective extraction methods have been chosen to identify the Fe, Mn, Al, Ca and OC phases. The Fe, Mn, and Al were measured in filtered solution (Whatman 41 filter, 20 µm size) by ICP-OES after the following extraction procedures: i) dithionite-citrate bicarbonate (DCB) (Mehra and Jackson, 1960), ii) ammonium oxalate in the dark 4h (oxalate) (Blakemore et al., 1981), and iii) sodium pyrophosphate (pyrophosphate) (Bascomb, 1968). In soils/sediments with a high pH, Ca could be an important contributor to the stabilizing mechanisms affecting OC (Rowley et al., 2018; Boiteau et al., 2020). Therefore, we measured Ca concentrations within the pyrophosphate extract. Extraction methods using DCB, oxalate and pyrophosphate are standard procedures to determine Fe- and Al-(oxyhydr)oxides phases or complexed ions (Supplementary Table S2). Here, we tested these extractions to decipher the different Mn phases. We found that the different extraction methods extracted different pools of Mn (Supplementary Figure S3). In addition, the Mn concentrations measured by ICP-OES on the solid residue after the different extractions support that DCB, oxalate and pyrophosphate extractions target different Mn pools. Repetitions (n = 3) for three different samples were conducted to assess

precision of the different methods (Supplementary Table S3). This analysis supports that these extractions can also be used to assess Mn pools.

Extraction with DCB is presumed to remove well crystalline, poorly crystalline Fe oxides and Fe complexed with organic matter from soil or sediment (Rennert, 2019), also called 'free iron'. Extraction with dithionite reduces Fe(III) from oxides. Similarly, Mn(IV) should be reduced to Mn(II) since Mn is redox-sensitive. The reduction of Mn(IV) is effective with hydroxylamine (NH_2OH), a weaker reductant than dithionite (Chao, 1972). Therefore, we assume that dithionite reduces Mn(IV) within Mn-oxides as well. Substantial amounts of Al and Ca are released via dithionite without targeting specific Al or Ca pools. The released Fe(II), Mn(II) and Al^{3+} and Ca^{2+} ions remain in solution and complexes with citrate (complexing agent).

Extraction with oxalate at pH 3 targets poorly crystalline oxides and complexed forms. At pH < 3.5, oxides are protonated weakening the metal-O bond, which is the first stage of dissolution, followed by the adsorption of oxalate and release of complexed Fe^{3+} and Al^{3+}. The oxalate extraction (4h in the dark procedure) is a rate-limited process, which targets poorly crystalline phases and complexed metals while longer procedures target more crystalline phases (Rennert, 2019). Unlike in the DCB extraction, several Al-containing minerals are dissolved by oxalate. These include hydroxyl-interlayer Al, poorly crystalline Al oxides, allophane, imogolite and other poorly crystalline aluminosilicates (Rennert et al., 2019). We emphasize that oxalate-extracted Ca cannot be discussed because of the precipitation of Ca with oxalate upon extraction.

Pyrophosphate extraction at pH 10 chelates polyvalent cations and therefore targets metals (Fe, Mn, Al and Ca) complexed with organic species. It has been reported that Na-pyrophosphate does not only target organically bond Fe but may also include nanoparticulate poorly crystalline Fe oxides (Regelink et al., 2014). Therefore, the release of Fe and Al from small particles that have not complexed with soil organic acids is not excluded during pyrophosphate extraction (Rennert, 2019).

The well crystallized (DCB-extracted) oxides are less reactive towards organic compounds because they offer less specific surface area than poorly crystalline oxides (Cornell and Schwertmann, 2003; Gentsch et al., 2015a). Moreover, DCB-extracted Al cannot be attributed to distinct Al minerals and does not target well-crystalized Al-oxides (Rennert, 2019). Dithionite-extraction was also reported to be unexpectedly less efficient within some permafrost soils (Jakobsen et al., 1996). Because it is difficult to decipher which phases are extracted by using DCB extraction method, we define our "reactive" pool (i.e., the pool highly reactive towards organic species) by the pool extracted by ammonium-oxalate. This pool should combine all poorly crystalline, amorphous and complexed pools of Fe, Mn and Al. Similarly, we define our reactive Ca as the pyrophosphate extracted Ca because of the drawback related to Ca oxalate precipitation and should include Ca under complexed forms or interacting via cation bridging.

Organic carbon was quantified in oxalate extract and in pyrophosphate extract. The optical density of oxalate extract (ODOE), considered as an indicator of reactive polyaromatic acid concentration, was measured by determining the absorbance at 430 nm on a Genesys 10 S VIS spectrophotometer, with the ammonium oxalate reagent as a blank (Daly, 1982). Note that the direct measurement of OC within oxalate extract is not possible because of the organic composition of oxalate. From the pyrophosphate extract, the concentration in dissolved OC released after dispersion by pyrophosphate (referred as Cp) was measured using a Shimadzu total organic carbon (TOC) analyzer (measuring non-purgeable OC). This indicates the amounts of C participating in organo-metallic complexes in soils or sediments (Bascomb, 1968). Repetitions (n = 3) for three different samples were conducted to assess the precision of the method (Supplementary Table S3).

3.3 Statistical analysis

The Wilcoxon-test (two-sided) was used to assess statistical differences within reactive metals and organic compounds (C_p) between the different cores. In addition, correlation matrices using Pearson method were constructed using *corrplot* package, performed with R software version 4.1.1 (R Core Team, 2018).

4 Results

4.1 Sediment core pH and mineralogy

The pH-H_2O ranged between 8.22 and 10.05 with a mean of 8.97 and pH-KCl ranged between 7.61 and 8.73 (mean = 8.18) (Supplementary Figure S4). Diffractograms indicate the presence of quartz, plagioclase, mica, pyroxene, amphibole, dolomite, serpentine and vermiculite (Supplementary Table S4). Mineral phases below 5% may be present but undetected.

4.2 Total and selectively extracted Fe, Mn, Al and Ca concentrations in sediment cores

The mean (± standard deviation) total concentrations in Fe, Al and Mn among all studied sediment cores are 26.1 ± 4.9 g kg^{-1}, 64.5 ± 5.2 g kg^{-1} and 0.50 ± 0.10 g kg^{-1}, respectively. Total Ca concentration reaches 23.6 ± 6.8 g kg^{-1}. Total Al concentration is 2-3 times higher than Fe concentrations and more than two orders of magnitude higher than Mn concentrations on mass concentration basis. The DCB-extracted Fe (mean: 5.41 g kg^{-1}) is almost one order of magnitude greater than DCB-extracted Al (mean: 0.63 g kg^{-1}) which is about two times greater than Mn (mean: 0.28 g kg^{-1}). Reactive Fe, Mn and Al (defined here as the oxalate-extracted pool) represent about ~12% (3.3 g kg^{-1}), 28% (0.15 g kg^{-1}) and 1.3% (0.85 g kg^{-1}) of the bulk total concentration, respectively (Figure 4a). Finally, pyrophosphate-extracted Fe represents ~3% (0.82 g kg^{-1}) of total Fe. Pyrophosphate-extracted Mn (0.13 g kg^{-1}) and Al (0.10 g kg-1) concentrations are smaller compared to Fe but falls within the same order of magnitude and represents ~25% and 0.2%, respectively of total Mn and total Al (Figure 4b). Pyrophosphate-extracted Ca shows the highest concentration with a mean of 3.5 g kg^{-1}.

When focusing on the differences in the selective extractions between the four stages of thermokarst formation (Figure 2), we found that reactive (i.e., oxalate-extracted) Fe concentrations show a significant increase between Yedoma and Alas deposits (Wilcoxon test p-value <0.05) but similar concentrations between dry and lake cores (p-value = 0.19). Similarly, reactive Mn shows significantly higher concentrations in the Alas compared to Yedoma core but significantly higher concentrations in dry deposits compared to lake deposits (Figure 5b). Reactive Al concentrations show a similar trend to reactive Mn, with higher concentrations in Alas cores compared to Yedoma cores and higher concentration in dry deposits than in lake deposits. Mean reactive Mn and Al concentration is therefore the lowest in the Yedoma lake core and the highest in the Alas dry core. Oxalate-extracted Al concentration is higher than DCB-extracted Al (Figure 5c). Pyrophosphate-extracted Fe showed smaller concentrations in the Yedoma dry and Yedoma lake cores (mean: 0.41 g kg^{-1} and 0.35 g kg^{-1}) compared to the Alas dry and Alas lake cores (mean: 1.5 g kg^{-1} and 1.6 g kg^{-1}). This difference between Yedoma and Alas sediments is smaller for Mn and Al concentrations within pyrophosphate extraction (Figure 5). Pyrophosphate-extracted Mn concentrations are within the same order of magnitude as pyrophosphate-extracted Al (mean: 0.13 g kg^{-1} and 0.10 g kg^{-1}, respectively; Figure 4a) despite the huge difference (more than two orders of magnitude) in the bulk Al and Mn total concentrations in the sediments (Figure 5). Pyrophosphate-extracted Ca ranges from 0.542 and 6.86 g kg^{-1} with mean values decreasing from Alas dry (4.40 g kg^{-1}), Alas lake (4.26 g kg^{-1}), Yedoma dry (3.06 g kg^{-1}) to Yedoma lake (2.89 g kg^{-1}) cores. Pyrophosphate-extracted Ca concentrations show higher values than the sum of pyrophosphate-extracted Fe, Mn and Al combined.

Detailed graphs of the Fe, Mn and Al concentrations over depth can be found in the Supplements: total, DCB, oxalate and pyrophosphate extractions (Figure S5-S7), and total and pyrophosphate extracted Ca

(Figure S8). Overall, DCB-, oxalate- and pyrophosphate-extracted Fe and Mn follow the same pattern as their total concentration profile. The Al total concentrations are two to three orders of magnitude higher than the concentration of selectively extracted Al. The sandy layer present in the Yedoma dry (between 19.3 and 10.1 m b.s.) is within the low range of values for all elements for their total, DCB-extracted, oxalate-extracted and pyrophosphate-extracted concentrations contributing to the greater variability (i.e., wider boxplot) within the Yedoma dry core (Figure 5). The total and selectively extracted Fe, Mn, Al and Ca concentrations are displayed in Supplementary Data.

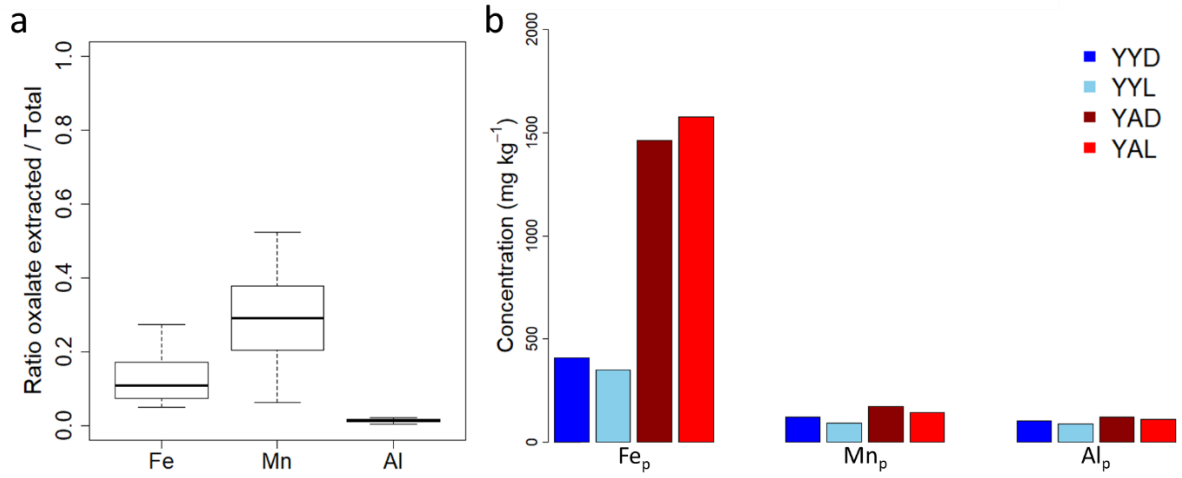

Figure 4. (a) Boxplot of the ratio between oxalate-extracted (i.e. reactive) and total Fe, Mn and Al. (b) Histogram of mean concentrations in pyrophosphate extracted Fe, Mn and Al in the four sediment cores: Yedoma dry (YYD), Yedoma lake (YYL), Alas dry (YAD) and Alas lake (YAL).

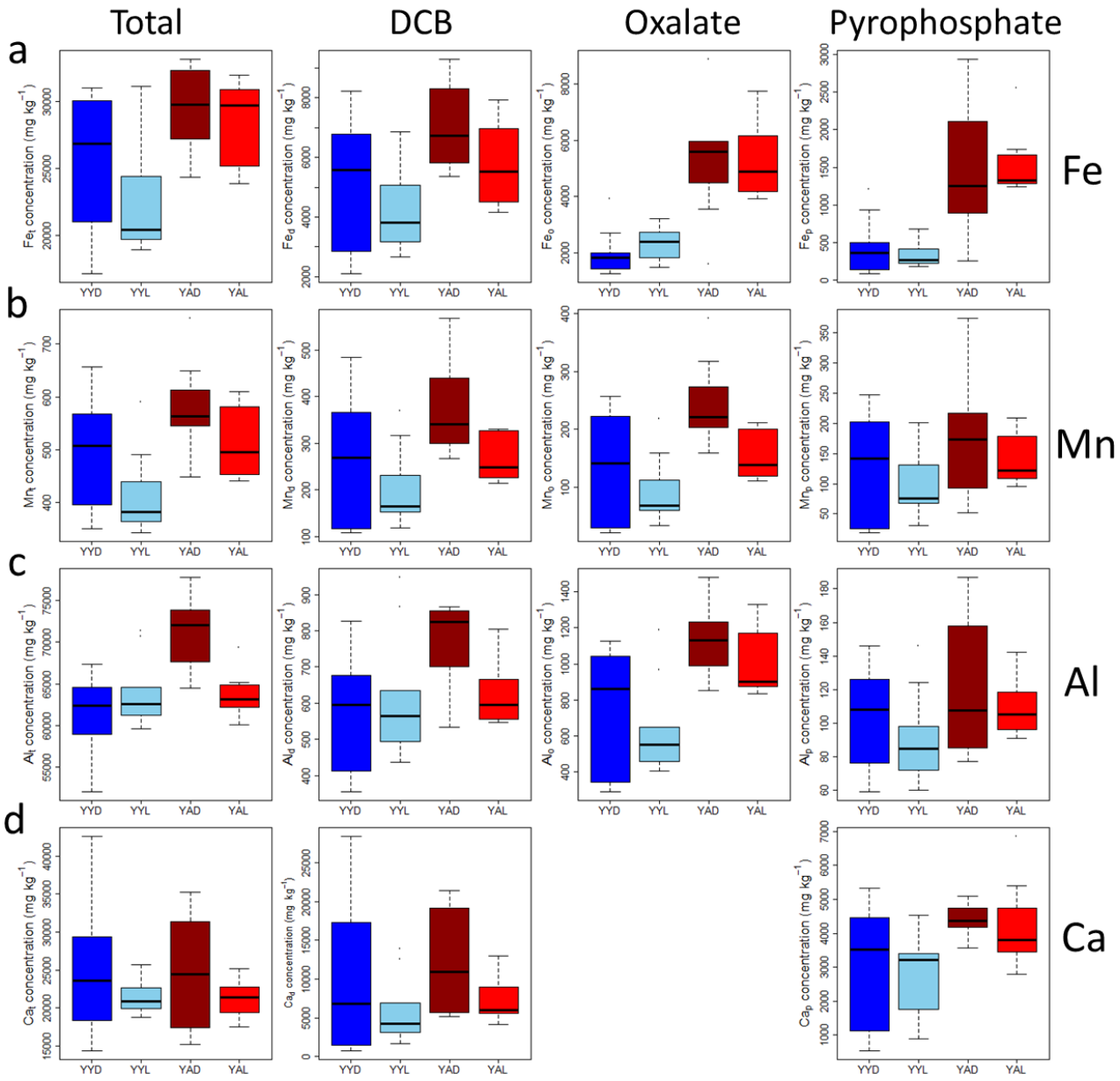

Figure 5. Boxplot of mineral element total concentrations and selectively extracted concentrations (expressed in mg kg^{-1}) using dithionite-citrate-bicarbonate (DCB), ammonium oxalate (oxalate) and Na-pyrophosphate (pyrophosphate) for (a) Fe, (b) Mn, (c) Al and (d) Ca for the four cores in Yukechi: Yedoma dry (YYD), Yedoma lake (YYL), Alas dry (YAD), Alas lake (YAL). Oxalate extraction of Ca is not shown due to precipitation issue (see methods Sect. 3.2.3). Yedoma cores are shown in blue and Alas cores in red. Indices are used for total, DCB, oxalate and pyrophosphate extracted metals, for instance in panel a, Fe_t, Fe_d, Fe_o and Fe_p, respectively. Note that the Y-scaling differs between plots for all elements.

4.3 Selective organic carbon extractions

Pyrophosphate-extracted C (C_p) concentration ranges are 2.2 - 15.4 g kg^{-1} (YYD), 1.6 - 6.6 g kg^{-1} (YYL), 4.1 - 9.2 g kg^{-1} (YAD) and 4.0 - 6.2 g kg^{-1} (YAL) (Figure 6a). Optical density of the oxalate extract (ODOE) ranges are 0.014 - 0.161 (YYD), 0.021 - 0.056 (YYL), 0.025 - 0.087 (YAD) and 0.049 - 0.106 (YAL) (Figure 6b). The Yedoma dry core shows the wider range of pyrophosphate-extracted C concentrations and Alas lake the narrower range (Figure 6a). Pyrophosphate-extracted C and optical density of the oxalate extract (ODOE) are positively correlated in the lower part of the Yedoma dry core ($R^2 = 0.52$), but not in the upper part (Supplementary Figure S9). The ODOE shows maximum values in the upper part of the Yedoma dry core. Notably, the sandy layer of the Yedoma dry core displays low

range values for pyrophosphate-extracted C and ODOE (Figure 6 and Supplementary Figure S9). Absorbance and concentrations for selective carbon extractions are displayed in Supplementary Data.

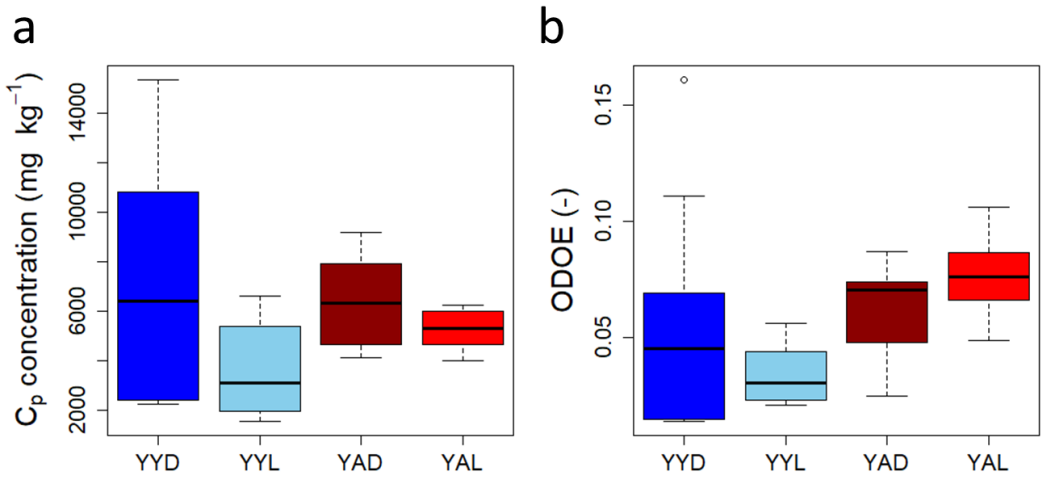

Figure 6. Boxplot of (a) pyrophosphate-extracted carbon concentration (C_p in mg kg^{-1}) and (b) optical density of the oxalate extract (ODOE) for Yedoma dry (YYD), Yedoma lake (YYL), Alas dry (YAD), and Alas lake (YAL) cores in Yukechi. Yedoma cores are shown in blue and Alas cores in red.

4.4 Statistical analysis of reactive metal and organic variables between stages of thermokarst process

Statistical analyses between the different cores highlight the significant differences occurring at each stage of the thermokarst process (Table 1). The initial lake formation (YYD to YYL; see Figure 3) triggered minor changes (not statistically significant; p-value > 0.05) in the concentration of the reactive metals (Fe_o, Mn_o, Al_o, Ca_p) and organic compounds (C_p and ODOE) (Table 1). The most significant differences during these stages are an increase in the concentration of reactive Fe phases and a decrease of complexed C (p-value slightly higher than 0.05 threshold). Note that the average concentration of complexed C decreases significantly (p-value <0.05) when the sandy sediments from the Yedoma dry core are discarded. In comparison, the drainage and refreezing stage (YYL to YAD; Figure 3) shows a statistically significant change for every parameter (p-value <0.05; Table 1): the concentration of all reactive metals (Supplementary Figure S10) and organic compounds (ODOE and C_p) increased significantly. The secondary thawing and mature lake formation (YAD to YAL; Figure 3) triggered only significant changes on the reactive Mn, but had no significant effect on reactive Fe and Al nor to OC parameters (Figure 5 and Table 1). In combination, the evolution from the Yedoma dry to the Alas dry (YYD to YAD) shows a significant increase in the concentration of reactive Fe, Mn and Al, and no significant change for the other parameters (e.g., ODOE and C_p). The shift from Yedoma (YYD and YYL) to Alas (YAD and YAL) modifies the concentrations of reactive Fe, Mn, Al and Ca (Table 1 and Supplementary Figure S10). However, the shift from dry deposits (YYD and YAD) towards deposits beneath lakes (YYL and YAL) only significantly affects reactive Mn and complexed C (Table 1; p-value<0.05). We found that all reactive metals are positively correlated with complexed C (Figure 7). Complexed Fe which is the most abundant after Ca (Fe_p mean: 0.82 g kg^{-1}) shows the smallest correlation with complexed C (r = 0.29). On the other hand, complexed Mn (mean around 0.13 g kg^{-1}), which is the least abundant along with Al, shows the highest correlation with pyrophosphate extracted C (r = 0.74).

Table 1. P-value table of Wilcoxon test (two sided) to decipher statistical significance of subsets for reactive metals and organic compounds. These reactive metals gather oxalate-extracted Fe, Mn and Al (Fe_o, Mn_o and Al_o) and pyrophosphate-extracted Ca

(Ca_p). Organic compounds are presented for optical density of the oxalate extract (ODOE) and pyrophosphate-extracted C (C_p). The p-values in bold character show statistical significant differences between the subsets. Subsets are the Yedoma dry (YYD), Yedoma lake (YYL), Alas dry (YAD) and Alas lake (YAL) cores. The (+) or (-) represents whether statistical differences is an increase or a decrease, respectively.

	Fe_o	Mn_o	Al_o	Ca_p	ODOE	C_p
*YYD vs YYL	0.0841	0.285	0.371	0.709	0.598	0.074
**YYL vs YAD	**<0.05 (+)**	**<0.05 (+)**	**<0.05 (+)**	**<0.05 (+)**	**<0.05 (+)**	**<0.05 (+)**
***YAD vs YAL	0.955	**<0.05 (-)**	0.336	0.336	0.148	0.397
****YYD vs YAD	**<0.05 (+)**	**<0.05 (+)**	**<0.05 (+)**	0.110	0.171	0.868
Yedoma vs Alas	**<0.05 (+)**	**<0.05 (+)**	**<0.05 (+)**	**<0.05 (+)**	**<0.05 (+)**	0.352
Dry vs Lake	0.190	**<0.05 (-)**	0.292	0.305	0.910	**<0.05 (-)**

*Initial lake formation effect (Figure 3c)
**Drainage and refreezing effect (Figure 3c)
***Second lake formation effect (Figure 3c)
**** Lake formation + drainage effects (combination of * and **)

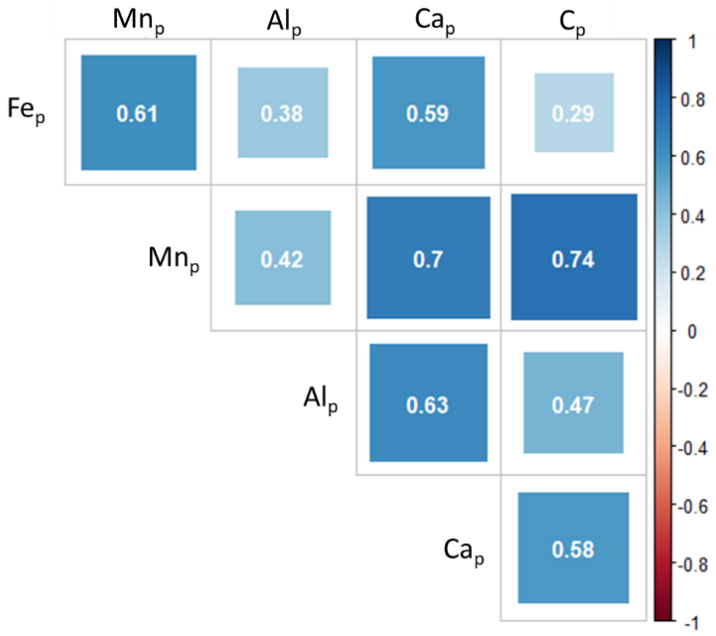

Figure 7. (a) Upper correlation matrix using Pearson method of complexed (pyrophosphate-extracted) metals and organic carbon (n = 39). Correlation matrix with all parameters, including total, dithionite-extracted, oxalate-extracted, pyrophosphate extracted metals and C is available in supplementary Figure S11.

5 Discussion

5.1 A typical Yedoma site modified by thermokarst process

Total mean Fe concentrations from all Yukechi cores (26.1 ± 4.9 g kg^{-1}, n = 39) are in the lower range of values compared to the median Fe concentration (31.7 ± 4.6 g kg^{-1}, n = 1,292) reported throughout the Yedoma domain (Monhonval et al., 2021b). However, total mean Al and Mn concentrations fall in the same concentration range (Al = 66.5 ± 6.9 g kg^{-1}; Mn = 0.498 ± 0.119 g kg^{-1}) as presented by Monhonval et al. (2020) in the Yedoma domain Mineral Concentration Assessment (YMCA) dataset. The total mean Ca concentration is twice as high (23.6 ± 6.8 g kg^{-1}) than the Yedoma domain median value (10.4 ± 4.7 g kg^{-1}, n = 1,292) (Monhonval et al., 2021a). Indeed, previous studies from Central

Yakutia showed that deposits in the area are rich in carbonates (Ulrich et al., 2019). This is further confirmed by the YMCA dataset (Monhonval et al., 2020), which highlights that Yukechi samples lie within the upper range of Ca concentration in Siberia (Supplementary Figure S12). The high pH values measured in Yukechi cores match previous findings from Central Yakutian lakes which exhibit a pH range of 7 to 10 (Pestryakova et al., 2012), and in unconnected Alas lakes from Central Yakutia with a pH > 9 (Hughes-Allen et al., 2021). Despite the fact that carbonate presence was undetected with X-ray diffraction method, reaction of the samples to HCl supports the presence of calcite or other carbonates (including Na_2CO_3 if sample pH is above 9), which were previously reported in the area (Ulrich et al., 2019). The carbonate presence within the Yukechi deposits, the high pH values reported within our four cores, and the high range total Ca concentration emphasize that Ca is likely to be an important contributor for mineral-OC interactions (Rowley et al., 2018; Sowers et al., 2020). Since redox and pH (to a lower extent) conditions can vary depending on the thawing history of deposits from each core, modifications in the contribution of each metal (Fe, Mn, Al, Ca) to mineral-OC interactions are expected.

To support the findings of this space-for-time study design, the following assumptions about the four stages of thermokarst development are made. Within typical Yedoma deposits, there is a uniform mineralogical composition (Strauss et al., 2017) and little post-depositional processing (Ulrich et al., 2021). Previous work from Schirrmeister et al., (2013, 2020) in the Yedoma domain support this assumption, showing that the Yedoma deposits originated from local sources and a variety of transport mechanisms, which resulted in a polygenetic formation of Yedoma deposits. We further assume that Alas deposits formed within and from Yedoma deposits and are mainly composed of re-located and re-worked Yedoma sediments (Schirrmeister et al., 2022), although authigenic deposition upon lake formation and drainage is expected. The uniform mineralogical nature of the Yukechi site is confirmed by the similarity of detected crystalline minerals from X-ray diffraction analyses within the original Yedoma dry cores and within the other three cores (Supplementary Table S4). The variety of transport mechanisms is confirmed by different grain-size distributions reported in previous studies (Ulrich et al., 2019, 2021; Windirsch et al., 2020). Therefore, we expect the main changes on mineral-OC interactions (i.e., Fe-, Mn-, Al-oxy(hydr)oxides and Fe, Mn, Al, Ca complexes and their associations to organic compounds) to be related to changing physico-chemical conditions in the sediment (i.e., redox state and pH), upon thermokarst processes and not related to a different composition of the original deposit. However, we acknowledge that spatial heterogeneity of the Yukechi site was not investigated and might explain part of the discrepancies observed in Yedoma and Alas deposits subjected to previous thaw. We acknowledge that additional factors not considered here such as the diversity of microbial communities (e.g., modulating CO_2:CH_4 ratio or oxide dissolution rates), the spatial and functional complexity in the sediment (e.g., the structuring of space into a network of more or less connected microsites that determine local environment conditions), or the catalyst role of mineral elements for organic reactions (e.g., through the creation of centre of reactivity, proton transfer or electron acceptor) may also contribute to influence mineral-OC interactions to some extent (Kleber et al., 2021).

5.2 Decoupling the influence of lake formation and lake drainage on mineral-organic carbon interactions

Biogeochemical conditions in the sediment (here referring to redox and pH) are modified during lake formation and lake drainage (Lipson et al., 2012). Lake formation and lake drainage may lead to contrasted physico-chemical conditions for OC stabilization and modify mineral-OC interactions. Indeed, mineral elements involved in mineral-OC interactions are either redox sensitive (Fe, Mn) and/or pH sensitive (Fe, Mn, Al, Ca). We assume redox conditions to change significantly beneath lakes or in dry deposits (Kögel-Knabner et al., 2010; Lipson et al., 2012). However, the pH measured within the four cores (dry and lake cores) display high values (around 8) without significant differences between cores, which complicates the observation of modifications for pH sensitive elements. Combining our

data of the four sediment cores, we are able to dissociate the impact of the following stages on mineral – OC interactions in the Yukechi sediments: i) the initial lake formation (modifications between the Yedoma dry and Yedoma lake cores); ii) the lake drainage and partial refreezing (modifications between the Yedoma lake and Alas dry cores); and iii) the second/mature lake formation (modifications between the Alas dry and Alas lake cores).

The difference in reactive Fe, Mn, Al across the sites of Yedoma and Alas show that there are opposing mechanisms upon lake formation and lake drainage. We demonstrate that the processes occurring during the intermediate steps are masked when comparing only the initial (YYD) and the final (YAD) deposits stage resulting from thermokarst processes. For instance, we observe that the combination of initial lake formation and drainage (YYD to YAD) shows no significant differences within the organic parameters concentrations (****; Table 1). Nonetheless, when considered separately, there is a decrease upon lake formation followed by an increase upon lake drainage for most parameters, including reactive metals, ODOE and C_p. We highlight that initial (*; Figure 3b) and secondary (***; Figure 3b) stages of lake formation had only minor effects on pedogenic Fe, Mn, Al, Ca but greater effects on OC phases (Table 1). On the other hand, drainage and refreezing (**; Figure 3b) of the Alas dry formation corresponded to a significant increase in reactive metal (Fe, Mn, Al, Ca) oxides and complexes and also a significant increase in ODOE and C_p. We can therefore state that reactive mineral formation and OC stabilization during drainage and refreezing outweighs any reactive mineral and organic carbon loss during the first thermokarst stage (i.e., initial lake formation). This finding supports that organic acid concentrations are unchanged between the Yedoma dry and the Alas dry (e.g., p-value = 0.87 for C_p). However, the intermediate stages involved in the formation of the Alas dry may have changed the form and properties of mineral-OC interactions from the original deposit with an increase in the potential to stabilize OC. Consequently, the Alas dry core contained the largest pool size of DCB-extracted Fe and Mn, and the highest reactive Fe and Mn proportion within this pool (Figure 8). More specifically, the size of the DCB-extracted pool increased about 36% for both Fe and Mn between the Yedoma dry and the Alas dry core. Reactive (amorphous and complexed) Fe increased from 37% to 75% and Mn increased from 51% to 65% out of the DCB-extracted pool (Figure 8).

The proportion of crystalline, amorphous and complexed Fe and Mn phases evolves with lake formation and lake drainage (Figure 8). Between the least degraded (Yedoma dry; YYD) and the more degraded core (Alas lake; YAL), the total DCB-extracted pool is relatively unchanged (increase of 11% for Fe and decrease of 1.5% for Mn). However, if we look at the distribution of Fe and Mn between the reactive phases, we observed some differences. Firstly, for Fe, the proportion of the complexed Fe phases increase by threefold and the amorphous Fe phases double at the expense of the proportion of crystalline phases which drops significantly (63% of the dithionite-extracted pool in Yedoma dry to 8% in the Alas lake). More specifically, in the least degraded Yedoma dry core, the majority of the DCB-extracted Fe is present as crystalline phases (63%) followed by amorphous pool (29%) and complexed phases (8%) (Figure 8). The Alas lake sediment core shows a very distinct distribution of the different Fe pools with only 8% of the DCB-extracted Fe as crystalline phases and an increase to 65% of amorphous phases and 27% of complexed forms. Secondly, for Mn, the crystalline phases represent 50%, the amorphous only 5.5% and complexed forms 44.5% of the DCB-extracted pool in the Yedoma dry core. The Alas lake shows a small depletion of crystalline phases (42%), amorphous phases stay unchanged (5%) and complexed forms increase (53%) in the DCB-extracted Mn pool (Figure 8). Overall, this supports a significant shift towards less crystalline and more reactive (amorphous and complexed) Fe compounds between the initial and the final step considered, and only a slight shift for reactive Mn compounds.

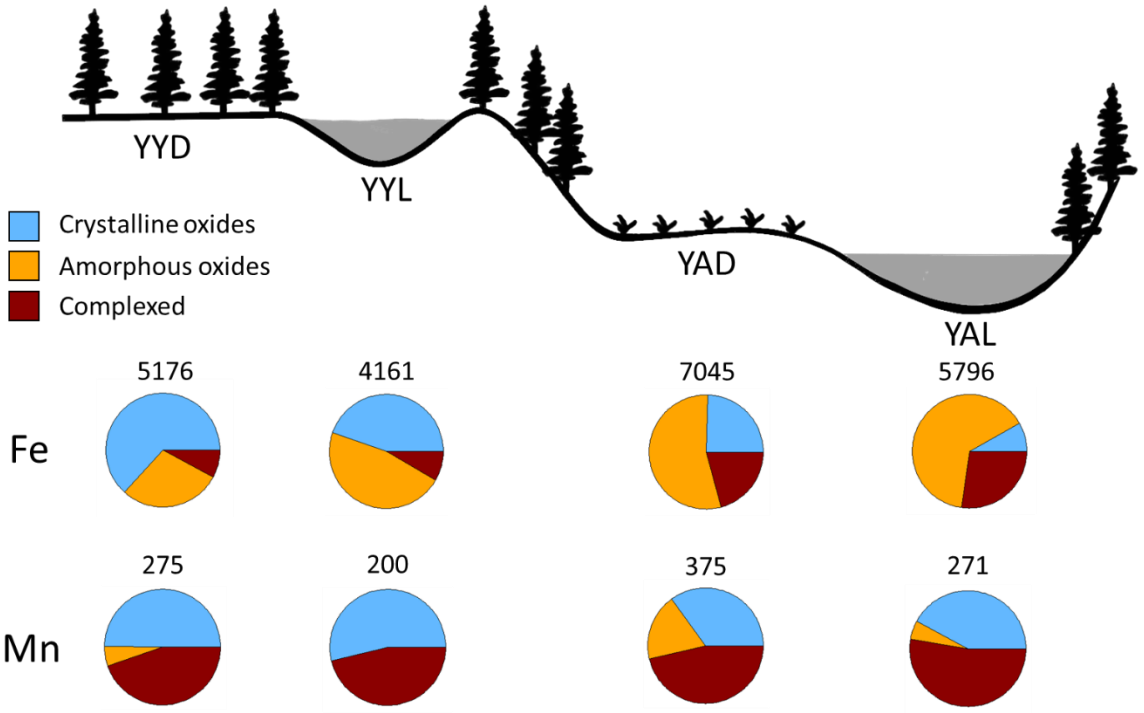

Figure 8. Proportion of crystalline oxides, amorphous oxides and complexed forms of Fe and Mn out of the oxide and complexed pool within the sequence of Yukechi cores. These values are based on selective extractions assuming crystalline oxide pool is the difference between DCB and oxalate-extracted and amorphous oxide pool the difference between oxalate and pyrophosphate-extracted. Complexed metals are pyrophosphate extracted. From left to right, cores represent the Yedoma dry (YYD), Yedoma lake (YYL), Alas dry (YAD) and Alas lake (YAL). The size of the total DCB-extracted pool, average in mg kg^{-1}, is given above each pie charts. The Al cannot be represented on the same basis because of higher proportion of oxalate-extracted Al than DCB-extracted Al.

The decrease of reactive Mn upon lake formation (Figure 5b), which is not the case for reactive Fe (Figure 5a), was not expected. Indeed, their similar properties related to redox sensitivity would suggest that both reactive Mn and Fe would increase upon oxidative conditions and decrease upon reductive conditions. We propose that the water saturation of Alas deposits beneath the lake might have decreased the redox potential only to a certain extent. To support this idea, Hughes-Allen et al. (2021) observed a decrease in dissolved O_2 to below 5% during winter in the bottom of shallow (~2 m deep) unconnected lakes from Central Yakutia (located less than 100 km apart and with very similar properties as the lakes overlying Yedoma and Alas lake cores from this study). The depleted oxygen levels beneath those lakes is additional evidence for a lower redox potential in the below-lake deposits discussed here. According to the redox ladder (Figure 1), Mn species are thermodynamically more favourable to reduce before Fe reduction. This means that Mn is theoretically reduced before Fe species upon reduction and Fe should be oxidized before Mn species upon oxidation (Patrick Jr. and Jugsujinda, 1992; Kappler et al., 2021). As a consequence, reduction of Mn minerals may be spatially separated from reduction of Fe minerals (for example, in stratified lake sediments) (Kappler et al., 2021). The potential Mn reduction upon lake formation might have a protective effect towards Fe reduction and prevent reactive Fe decrease upon lake formation as observed here (Figure 4a). However, in many environments Mn cycling and Fe cycling are tightly coupled, where steep redox gradients exist on small scales (Kappler et al., 2021). Our data could be evidence for the preferential dissolution of Mn phases (relative to Fe phases) upon thermokarst lake formation.

Currently the increase in the number of lakes across the Circum-Arctic region is not offsetting the land area gained through lake drainage: this is suggesting that the transition from lake to drained thaw lake basins (i.e. Alas) is leading to permafrost aggradation and increasing carbon sequestration (Jones et al.,

2022). However, future warming, reduced freezing and potential second lake formation may have a disruptive effect in this trajectory (Jones et al., 2022). Lake formation and lake drainage, and their intermediaries, are therefore highly relevant stages of permafrost condition today and in the future. We investigate the influence of the end-stages and intermediate stages of thermokarst processes on Fe- and Mn-OC interactions and show that drainage and refreezing triggered the increase in absolute and relative concentration of reactive Fe and Mn phases. In addition, the pool of reactive minerals is higher within the Alas lake than the Yedoma lake core suggesting an increase in mineral-OC interactions. This suggests that secondary lake formation would have smaller impact on OC release and subsequent mineralization than initial lake formation. In summary, the increase of reactive Fe and Mn (poorly crystalline oxides and complexes) at the expense of well crystalline oxides from Yedoma to Alas cores is likely beneficial for OC stabilization (Wagai et al., 2013; Chen et al., 2014; Kleber et al., 2015).

5.3 Changing organo-metallic bindings with the thawing history of ice-rich permafrost deposits

The molar contribution of Ca, Fe, Al and Mn out of the sum of the complexed phases differs for each metal. On average, this contribution decreases following the sequence Ca, Fe, Al and Mn with 80.7%, 13.5%, 3.6%, and 2.2% of contribution, respectively. The high contribution of a metal (quantitatively) out of the total complexed metal pool is not the only criterion to prove that this metal is the most influential (qualitatively) on OC binding and protection. Within sediments (all characterized by high pH), we found that Ca is the dominant contributor for organo-metallic complexes. The high Ca concentration within these deposits and the poor solubility of Fe(III) under circumneutral pH might explain the higher contribution of Ca compared to Fe. However, organo-metallic complexes can involve both Fe(II) and Fe(III) and the reported co-occurrence of Fe(II) and Fe(III) in organic complexes from both oxic and anoxic sediments can explain the substantial role of Fe despite the alkaline pH and reductive conditions within sediments (Bhattacharyya et al., 2018). Additionally, we found a strong correlation between Mn_p (a minor player quantitatively compared to Fe_p or Ca_p) and C_p (Figure 7), which emphasizes that Mn is likely an important player qualitatively to form association with C and increase its stabilization.

The saturation of functional groups within soluble organic acids can be approached by the metal:C molar ratio, i.e., the ratio between the sum of pyrophosphate-extracted metals (Fe_p, Mn_p, Al_p and Ca_p) and pyrophosphate-extracted C (C_p) (Stevenson, 1994; Nierop et al., 2002; Schwesig et al., 2003). As described by Boudot et al. (1989), organo-metallic complexes which exhibit a low metal:C molar ratio are easily biodegraded because of the lack of significant protective effect. In short, the higher the metal:C molar ratio, the better protected the organic matter may be against microbial degradation. In the Yedoma dry core (YYD), the metal:C molar ratio is around 0.1. Upon thermokarst process, this molar ratio increases and all other cores (YYL, YAD, YAL) display a metal:C molar ratio around 0.3 (Figure 9). Organic acids display thus fewer bindings with metals within the Yedoma dry core compared to other cores. The initial lake formation led to a depletion in complexed C and to a lesser extent in complexed metals (Figure 9b, arrow 1) with a significant shift from metal:C molar ratio from 0.1 to 0.3 ratio line (Figure 9a). The second stage of the thermokarst process (i.e., drainage and refreezing; Figure 9b, arrow 2) led to an increase of both complexed C and complexed metals following the 0.3 ratio line. Finally, the second lake formation had no or few effects on C and metal molar concentrations compared to the initial lake formation. Complexation between organic acids and metals lowers the solubility of organic acids and hence its availability to microorganisms (Baldock and Skjemstad, 2000). This, in turn, can decrease the susceptibility to biological attack and hinders mineralization of organic molecules (Oades, 1988). Two hypotheses can explain an increase in metal:C molar ratio: i) the density of functional groups is constant and the quantity of metals binding to these functional groups is increasing, or ii) polyfunctional groups are saturated with metal cations but the density of polyfunctional groups is increasing. The abundance of metals cations (especially Ca) suggests that functional groups are likely

saturated, and that the second hypothesis is more likely. Either way, the increase in metal:C ratio results in increasing protection for organic acids. Therefore, the increased metal:C ratio observed after thawing of the Yedoma dry deposits likely results in the increase of stability inferred from complexation between metals and OC and to the previous loss of unprotected OC.

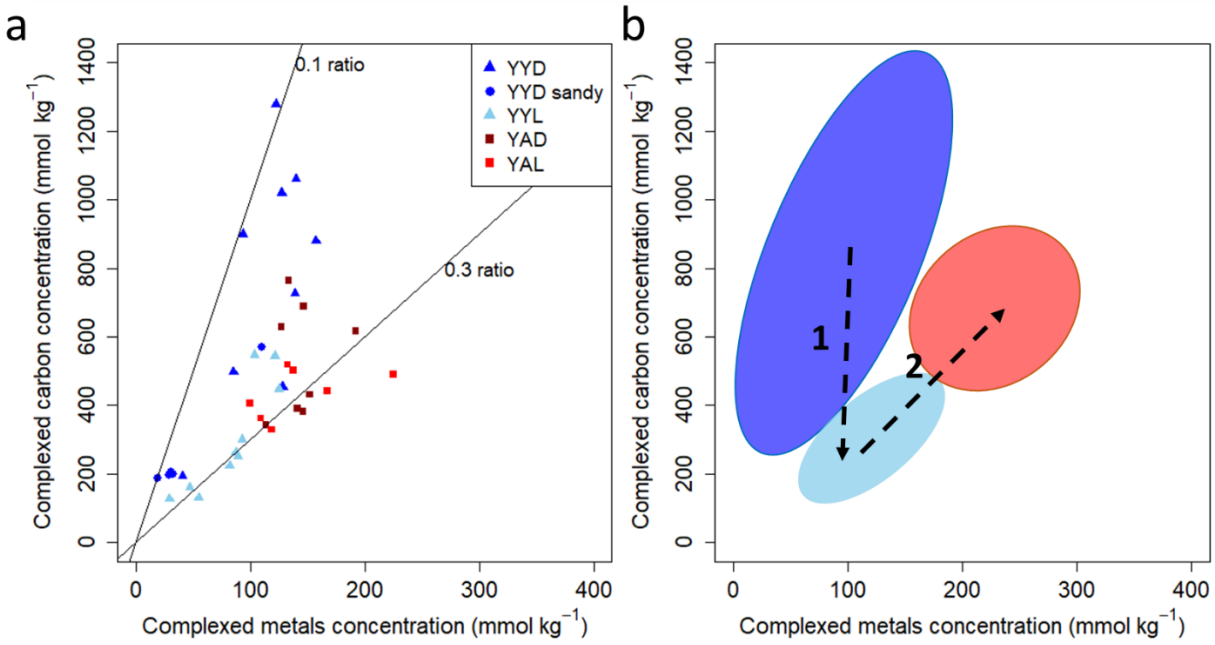

Figure 9. a) Relation between the concentration (in mmol kg^{-1}) of complexed carbon (y-axis) and the sum of complexed metals (including Fe, Mn, Al and Ca) for Yedoma dry (YYD), Yedoma lake (YYL), Alas dry (YAD) and Alas lake (YAL) cores. b) conceptual view of the influence of lake formation (1) and lake drainage (2) on complexed mineral and organic phases.

Dissolved organic acids have a high density of carboxyl groups (on average one carboxyl group for every ten C atoms; pKa around 4-5) (Stevenson, 1994). For acidic pH, where we found a dominance of carboxylic polyfunctional group (Catrouillet et al., 2014), organic acids are thus considered saturated around a metal:C molar ratio of 0.1. Here, the high pH (mean around 8-9) allows the presence of other functional groups such as phenolic groups (pKa around 10) (Bell, 2013). Advanced stages of organic matter degradation and subsequent depolymerization and oxidation can also lead to the increase of abundance of polar functional groups and enhance their chemical reactivity towards metal cations and mineral surfaces (Kleber et al., 2021). Polyvalent cations (i.e., $Fe^{3+/2+}$, Al^{3+}, $Mn^{4+/3+/2+}$ and Ca^{2+}) can bind via coordination to those multiple functional groups and form stable organo-metallic complexes. Complexation mechanisms maintain OC stability and slow down its decomposition rate (Chen et al., 2022). The increase in metal:C ratio after thawing highlights the increase of metal-C coordination bindings and suggests a higher protective role against microbial mineralization.

5.4 Implications for greenhouse gases emissions

We have the excellent opportunity to combine data on mineral-OC interactions presented in this study with incubation experiments quantifying CO_2 and CH_4 emissions from identical Yedoma lake and Alas lake sediment cores (Jongejans et al., 2021b). The cumulative greenhouse gas production after 1 year of incubation was the highest in Yedoma lake sediments, and was 3 and 1.5 times lower in Alas lake sediments for CO_2 and CH_4, respectively (Jongejans et al., 2021b). The authors concluded that the highest production in Yedoma deposits was likely due to the decomposition of readily bioavailable organic matter, and that the lower greenhouse gases production in the non-frozen Alas lake sediments

likely resulted from advanced OM decomposition during Holocene talik development. Higher greenhouse gas emissions were reported in the Yedoma lake core despite the lower total OC content within this core (median YYL: 0.5 wt%) relative to the Alas lake core (median YAL: 0.8 wt%).

We suggest that the increase in stabilizing mechanisms (involving reactive Fe, Mn, Al, and Ca) in the Alas lake core compared to the Yedoma lake core (Figure 8) could also explain the lowest greenhouse gas production in Alas lake sediments (Figure 10). The lower CO_2 and slightly lower CH_4 production (Figure 10a and Figure 10b, respectively) in the Alas lake core relative to the Yedoma lake core is concomitant with an increase of both complexed C and sum of complexed metals concentrations (Figure 10). In addition, the increase in reactive Fe (Fe_o/Fe_t; Figure 10), and reactive Mn, Al and Ca after first lake drainage (Mn_o/Mn_t, Al_o/Al_t, Ca_p/Ca_t; Supplementary Figure S13) likely offers better protection for the OC in the sediment. There is also an increase in the total amount of stabilized complexed C upon the drainage process, a pool that is kept during the second lake formation (Figure 9b, arrow 2). All of these would contribute to the decrease of CO_2 and CH_4 emissions in Alas lake sediments relative to the Yedoma lake sediments. Quantitatively, metals participating in organo-metallic complexes increased by ~70% in the Alas lake relative to the Yedoma lake (83 mmol kg^{-1} in YYL to 141 mmol kg^{-1} in YAL; Figure 10) and may hinder the efficacy of microbial enzymes to degrade OC (Mikutta et al., 2006; Kleber et al., 2007). The amounts of poorly crystallized Fe oxides (Fe_o-Fe_p) almost doubled, from 1.96 g kg^{-1} in the Yedoma lake to 3.74 g kg^{-1} in the Alas lake, on average. Thanks to the high specific surface area of poorly crystallized oxides, iron oxy(hydr)oxides can sorb up to 0.22 g OC g Fe^{-1} (Wagai and Mayer, 2007). Based on this ratio, Yedoma lake sediments can sorb and protect up to 0.83 g OC kg^{-1} (mean YYL: 3.81 g Fe kg^{-1}) and Alas lake sediments up to 0.93 g OC kg^{-1} (mean YAL: 4.22 g Fe kg^{-1}), which represents a 12% increase.

Overall, we suggest that the shift in the proportion of reactive Fe (from 10.4% in Yedoma lake to 18.6% in Alas lake) and of reactive Mn (from 21.2% in Yedoma lake to 30% in Alas lake) out of their total concentration (also true for reactive Al and Ca; Supplementary Figure S14) might contribute to mitigate CO_2 and CH_4 emissions. In addition, the increased availability of Fe and Mn within the Alas lake core can promote anaerobic oxidation of CH_4 (AOM) (Lipson et al., 2012; Miller et al., 2015, 2019). Under anaerobic conditions, a variety of microorganisms are capable of using Fe and Mn to oxidize CH_4 and mitigate CH_4 emissions (Blodau, 2002; Beal et al., 2009). The decrease in CH_4 production within the Alas lake core could be explained by an increase in reactive Fe and Mn. Further investigations are still needed to quantify the direct impact of such mineral OC interactions on methane production rates.

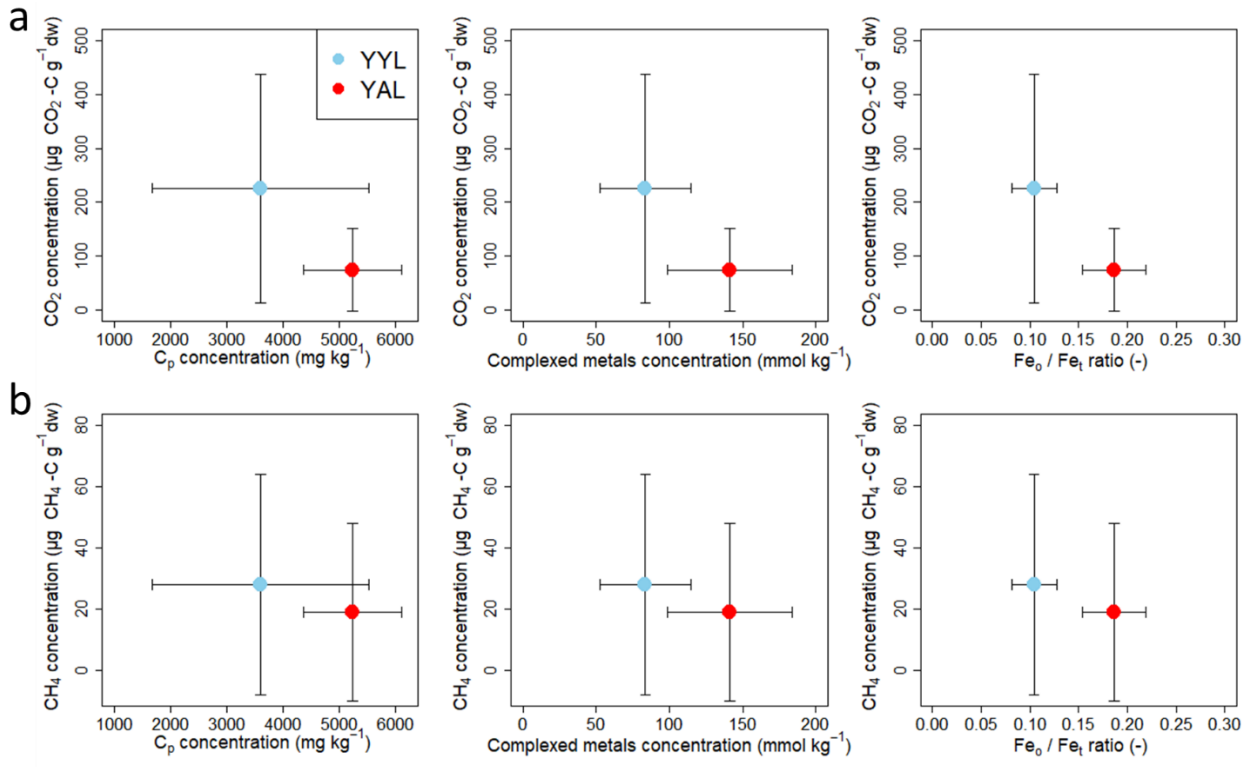

Figure 10. Mean and standard deviation of (a) CO_2 (expressed in µg CO_2-C g^{-1} dry weight) and (b) CH_4 (expressed in µg CH_4-C g^{-1} dry weight) emissions on the y-axis and mineral stabilization parameters (pyrophosphate extracted C, sum of complexed metals concentration and Fe_o/Fe_t ratio) on the x-axis for the Yedoma lake sediments (YYL, blue) and the Alas lake sediments (YAL, red). The mean greenhouse gases (CO_2 and CH_4) concentration values are from one-year long (4°C, dark) incubation experiments for Yedoma lake sediments (YYL; n = 7) and Alas lake sediments (YAL; n = 10)(Jongejans et al., 2021b). No incubation experiments are available in the Yedoma dry and Alas dry sediments to compare with the other cores.

In combination, sediment incubation data and mineral-organic carbon characterization validate the increased attention given to mineral-OC interactions for their potential influence on the permafrost carbon feedback. We demonstrate that the increased abundance in stabilizing surfaces and ions (i.e., via adsorption, co-precipitation, complexation) led to the decrease in microbial degradation and potentially to methanogenesis inhibition. While many other parameters can influence greenhouse gas emissions (carbon quality, quantity, microbial community diversity), we claim that mineral-OC interactions cannot be neglected. Incubation experiments highlighted the contribution and importance of organo-mineral associations for soil OC sequestration in soils of the Siberian Arctic, with over 50% of soil OC bound to minerals (Gentsch et al., 2015a). The potential to increase CO_2 and CH_4 production in ecosystems vulnerable to thermokarst processes could be limited by the increase of reactive metals that enhance OC protection and by the increase of Fe and Mn availability that may inhibits CH_4 production (Bodegom et al., 2004; Lipson et al., 2012). Our data support the overwhelming evidence that mineral-OC interactions are key for a more comprehensive understanding of potential greenhouse gases emissions upon recent and future thermokarst processes.

6 Conclusion

This study investigated the role of the reactive metals Fe, Mn, Al and Ca in mineral-organic carbon interactions along a landscape transect in Central Yakutia from undisturbed Yedoma uplands to drained lake and thermokarst lakes sediments from different generations. We quantified the influence of thermokarst lake formation and drainage on mineral-OC interactions. Our main conclusions are the following:

(i) Intermediate stages of thermokarst processes like lake formation and lake drainage largely influence interactions between reactive metals and OC. Lake formation decreased the amount of complexed OC by 50% and reactive Mn phases by 33%. Lake drainage (disappearance) and refreezing substantially increased the amount of organic compounds (complexed OC and associated to mineral surfaces) and all reactive metals (Fe, Mn, Al, Ca). The maximum of reactive metals is found within the Alas dry core (YAD).
(ii) Upon the range of thermokarst process here considered (Yedoma dry (YYD) to Alas lake sediments (YAL), the amount of complexed Fe phases increases by threefold. The amount of amorphous Fe doubles at the expense of crystalline phases which drop significantly from the Yedoma dry to the Alas lake core (63% of crystalline Fe oxides in the free iron pool in the Yedoma dry (YYD) and 8% in the Alas lake (YAL)). Despite a significant increase of amorphous and complexed Mn concentrations in the Alas dry core (YAD), the amount of reactive Mn remains relatively similar from Yedoma dry (YYD) to Alas lake core (YAL). Reactive Al and Ca concentrations increase significantly with the thermokarst lake drainage whereas lake formation has only minor influence with a slight decrease in reactive Al and Ca concentrations.
(iii) Following thermokarst processes, organic carbon has more opportunity to bind with metal cations which likely increases the stability of organic matter and mitigate microbial degradation.
(iv) The higher proportion of reactive metals and complexed organic carbon in Alas lake deposits (YAL) than in Yedoma lake deposits (YYL) is concomitant with lower CO_2 and CH_4 emissions reported in Alas than in Yedoma deposits from the same cores via incubation experiments.

We found an increase in the supply of stabilizing Fe, Mn and Al surfaces, especially Fe-oxy(hydr)oxides and Fe, Mn, Al, Ca cations providing an increasing protection for OC. We found an increase in poorly crystalline oxides and in metal:C bindings within organo-metallic complexes upon thermokarst lake drainage and refreezing. All of these contributed to the concomitant decrease of CO_2 and CH_4 emission upon secondary thawing of Alas deposits. Overall, our data emphasize the overwhelming evidence that mineral-OC interactions need to be considered in the estimates of future greenhouse gases emissions upon thawing of ice-rich permafrost deposits.

7 Author contributions

AM and SO conceived and planned the experiment work. AG and JL conducted the pXRF and XRD measurements and selective extractions with the help of AM. EBA conducted pH analysis. JS, LLJ, LS, GG and MU provided the samples and contributed with their expertise on permafrost stratigraphy and the sedimentological history of the sample deposits. HT, CH, and MT contributed with their expertise on metals in permafrost regions. BP and AV helped with pXRF methodology. AM, AG and JL performed the data processing. AM wrote the manuscript with inputs from all co-authors.

8 Data availability statement

The data that supports the findings of this study are available in the supplementary material of this article.

9 References

Baldock, J.A., Skjemstad, J.O., 2000. Role of the soil matrix and minerals in protecting natural organic materials against biological attack. Org. Geochem. 31, 697–710. https://doi.org/10.1016/S0146-6380(00)00049-8

Barber, A., Brandes, J., Leri, A., Lalonde, K., Balind, K., Wirick, S., Wang, J., Gélinas, Y., 2017. Preservation of organic matter in marine sediments by inner-sphere interactions with reactive iron. Sci. Rep. 7, 366. https://doi.org/10.1038/s41598-017-00494-0

Bartlett, R.J., Ross, D.S., 2005. Chemistry of Redox Processes in Soils, in: Chemical Processes in Soils. John Wiley & Sons, Ltd, pp. 461–487. https://doi.org/10.2136/sssabookser8.c9

Bascomb, C.L., 1968. Distribution of Pyrophosphate-Extractable Iron and Organic Carbon in Soils of Various Groups. J. Soil Sci. 19, 251–268. https://doi.org/10.1111/j.1365-2389.1968.tb01538.x

Beal, E.J., House, C.H., Orphan, V.J., 2009. Manganese- and Iron-Dependent Marine Methane Oxidation. Science 325, 184–187. https://doi.org/10.1126/science.1169984

Bell, R.P., 2013. The Proton in Chemistry. Springer Science & Business Media.

Bhattacharyya, A., Schmidt, M.P., Stavitski, E., Martínez, C.E., 2018. Iron speciation in peats: Chemical and spectroscopic evidence for the co-occurrence of ferric and ferrous iron in organic complexes and mineral precipitates. Org. Geochem. 115, 124–137. https://doi.org/10.1016/j.orggeochem.2017.10.012

Biskaborn, B.K., Smith, S.L., Noetzli, J., Matthes, H., Vieira, G., Streletskiy, D.A., Schoeneich, P., Romanovsky, V.E., Lewkowicz, A.G., Abramov, A., Allard, M., Boike, J., Cable, W.L., Christiansen, H.H., Delaloye, R., Diekmann, B., Drozdov, D., Etzelmüller, B., Grosse, G., Guglielmin, M., Ingeman-Nielsen, T., Isaksen, K., Ishikawa, M., Johansson, M., Johannsson, H., Joo, A., Kaverin, D., Kholodov, A., Konstantinov, P., Kröger, T., Lambiel, C., Lanckman, J.-P., Luo, D., Malkova, G., Meiklejohn, I., Moskalenko, N., Oliva, M., Phillips, M., Ramos, M., Sannel, A.B.K., Sergeev, D., Seybold, C., Skryabin, P., Vasiliev, A., Wu, Q., Yoshikawa, K., Zheleznyak, M., Lantuit, H., 2019. Permafrost is warming at a global scale. Nat. Commun. 10, 264. https://doi.org/10.1038/s41467-018-08240-4

Blakemore, L.C., Searle, P.L., Daly, B.K., 1981. Methods for chemical analysis of soils. New Zealand Soil Bureau Scientific Report 10 A, second revision 102. https://doi.org/10.7931/DL1-SBSR-10A

Blodau, C., 2002. Carbon cycling in peatlands — A review of processes and controls. Environ. Rev. 10, 111–134.

Bodegom, P.M., Scholten, J.C.M., Stams, A.J.M., 2004. Direct inhibition of methanogenesis by ferric iron. FEMS Microbiol. Ecol. 49, 261–268. https://doi.org/10.1016/j.femsec.2004.03.017

Boiteau, R.M., Kukkadapu, R., Cliff, J.B., Smallwood, C.R., Kovarik, L., Wirth, M.G., Engelhard, M.H., Varga, T., Dohnalkova, A., Perea, D.E., Wietsma, T., Moran, J.J., Hofmockel, K.S., 2020. Calcareous organic matter coatings sequester siderophores in alkaline soils. Sci. Total Environ. 724, 138250. https://doi.org/10.1016/j.scitotenv.2020.138250

Boudot, J.P., Hadj, A.B., Steiman, R., Seigle-Murandi, F., 1989. Biodegradation of synthetic organo-metallic complexes of iron and aluminium with selected metal to carbon ratios. Soil Biol. Biochem. 21, 961–966.

Catrouillet, C., Davranche, M., Dia, A., Bouhnik-Le Coz, M., Marsac, R., Pourret, O., Gruau, G., 2014. Geochemical modeling of Fe(II) binding to humic and fulvic acids. Chem. Geol. 372, 109–118. https://doi.org/10.1016/j.chemgeo.2014.02.019

Chao, T.T., 1972. Selective Dissolution of Manganese Oxides from Soils and Sediments with Acidified Hydroxylamine Hydrochloride. Soil Sci. Soc. Am. J. 36, 764–768. https://doi.org/10.2136/sssaj1972.03615995003600050024x

Chen, C., Dynes, J.J., Wang, J., Sparks, D.L., 2014. Properties of Fe-Organic Matter Associations via Coprecipitation versus Adsorption. Environ. Sci. Technol. 48, 13751–13759. https://doi.org/10.1021/es503669u

Chen, Q., Zhang, P., Hu, Z., Li, S., Zhang, Y., Hu, L., Zhou, L., Lin, B., Li, X., 2022. Soil Organic Carbon and Geochemical Characteristics on Different Rocks and Their Significance for Carbon Cycles. Front. Environ. Sci. 9.

Climate-data.org, 2022. Climate data for cities worldwide [WWW Document]. URL https://en.climate-data.org/asia/russian-federation/sakha-republic/yakutsk-1806/

Cornell, R.M., Schwertmann, U., 2003. The iron oxides: structure, properties, reactions, occurrences and uses. John Wiley & Sons.

Daly, B.K., 1982. Identification of podzols and podzolised soils in New Zealand by relative absorbance of oxalate extracts of A and B horizons. Geoderma 28, 29–38. https://doi.org/10.1016/0016-7061(82)90038-6

Davis, C.C., Edwards, M., 2017. Role of Calcium in the Coagulation of NOM with Ferric Chloride. Environ. Sci. Technol. 51, 11652–11659. https://doi.org/10.1021/acs.est.7b02038

Dutta, K., Schuur, E.A.G., Neff, J.C., Zimov, S.A., 2006. Potential carbon release from permafrost soils of Northeastern Siberia. Glob. Change Biol. 12, 2336–2351. https://doi.org/10.1111/j.1365-2486.2006.01259.x

Eglinton, T.I., 2012. A rusty carbon sink. Nature 483, 165–166. https://doi.org/10.1038/483165a

Ernakovich, J.G., Lynch, L.M., Brewer, P.E., Calderon, F.J., Wallenstein, M.D., 2017. Redox and temperature-sensitive changes in microbial communities and soil chemistry dictate greenhouse gas loss from thawed permafrost. Biogeochemistry 134, 183–200. https://doi.org/10.1007/s10533-017-0354-5

Eusterhues, K., Wagner, F.E., Häusler, W., Hanzlik, M., Knicker, H., Totsche, K.U., Kögel-Knabner, I., Schwertmann, U., 2008. Characterization of Ferrihydrite-Soil Organic Matter Coprecipitates by X-ray Diffraction and Mössbauer Spectroscopy. Environ. Sci. Technol. 42, 7891–7897. https://doi.org/10.1021/es800881w

Fiedler, S., Sommer, M., 2004. Water and Redox Conditions in Wetland Soils—Their Influence on Pedogenic Oxides and Morphology. SOIL SCI SOC AM J 68, 10.

Fiedler, S., Wagner, D., Kutzbach, L., Pfeiffer, E.-M., 2004. Element Redistribution along Hydraulic and Redox Gradients of Low-Centered Polygons, Lena Delta, Northern Siberia. Soil Sci. Soc. Am. J. 68, 1002–1011. https://doi.org/10.2136/sssaj2004.1002

Fritsch, E., Allard, T., Benedetti, M.F., Bardy, M., do Nascimento, N.R., Li, Y., Calas, G., 2009. Organic complexation and translocation of ferric iron in podzols of the Negro River watershed. Separation of secondary Fe species from Al species. Geochim. Cosmochim. Acta 73, 1813–1825. https://doi.org/10.1016/j.gca.2009.01.008

Gentsch, N., Mikutta, R., Alves, R.J.E., Barta, J., Čapek, P., Gittel, A., Hugelius, G., Kuhry, P., Lashchinskiy, N., Palmtag, J., Richter, A., Šantrůčková, H., Schnecker, J., Shibistova, O., Urich, T., Wild, B., Guggenberger, G., 2015a. Storage and transformation of organic matter fractions in cryoturbated permafrost soils across the Siberian Arctic. Biogeosciences 12, 4525–4542. https://doi.org/10.5194/bg-12-4525-2015

Gentsch, N., Mikutta, R., Shibistova, O., Wild, B., Schnecker, J., Richter, A., Urich, T., Gittel, A., Šantrůčková, H., Bárta, J., Lashchinskiy, N., Mueller, C.W., Fuß, R., Guggenberger, G., 2015b. Properties and bioavailability of particulate and mineral-associated organic matter in Arctic permafrost soils, Lower Kolyma Region, Russia: Organic matter stabilization in permafrost soils. Eur. J. Soil Sci. 66, 722–734. https://doi.org/10.1111/ejss.12269

Gorokhov, A.N., Fedorov, A.N., 2018. Current Trends in Climate Change in Yakutia. Geogr. Nat. Resour. 39, 153–161. https://doi.org/10.1134/S1875372818020087

Grant, K.E., Galy, V.V., Haghipour, N., Eglinton, T.I., Derry, L.A., 2022. Persistence of old soil carbon under changing climate: The role of mineral-organic matter interactions. Chem. Geol. 587, 120629. https://doi.org/10.1016/j.chemgeo.2021.120629

Grosse, G., Jones, B., Arp, C., 2013. 8.21 Thermokarst Lakes, Drainage, and Drained Basins, in: Treatise on Geomorphology. Elsevier, pp. 325–353. https://doi.org/10.1016/B978-0-12-374739-6.00216-5

Hemingway, J.D., Rothman, D.H., Grant, K.E., Rosengard, S.Z., Eglinton, T.I., Derry, L.A., Galy, V.V., 2019. Mineral protection regulates long-term global preservation of natural organic carbon. Nature 570, 228–231. https://doi.org/10.1038/s41586-019-1280-6

Herndon, E., AlBashaireh, A., Singer, D., Roy Chowdhury, T., Gu, B., Graham, D., 2017. Influence of iron redox cycling on organo-mineral associations in Arctic tundra soil. Geochim. Cosmochim. Acta 207, 210–231. https://doi.org/10.1016/j.gca.2017.02.034

Herndon, E., Kinsman-Costello, L., Godsey, S., 2020. Biogeochemical Cycling of Redox-Sensitive Elements in Permafrost-Affected Ecosystems, in: Dontsova, K., Balogh-Brunstad, Z., Le Roux, G. (Eds.), Geophysical Monograph Series. Wiley, pp. 245–265. https://doi.org/10.1002/9781119413332.ch12

Huang, W., Hall, S.J., 2017. Elevated moisture stimulates carbon loss from mineral soils by releasing protected organic matter. Nat. Commun. 8, 1–10. https://doi.org/10.1038/s41467-017-01998-z

Hugelius, G., Strauss, J., Zubrzycki, S., Harden, J.W., Schuur, E.A.G., Ping, C.-L., Schirrmeister, L., Grosse, G., Michaelson, G.J., Koven, C.D., O'Donnell, J.A., Elberling, B., Mishra, U., Camill, P., Yu, Z., Palmtag, J., Kuhry, P., 2014. Estimated stocks of circumpolar permafrost carbon with quantified uncertainty ranges and identified data gaps. Biogeosciences 11, 6573–6593. https://doi.org/10.5194/bg-11-6573-2014

Hughes-Allen, L., Bouchard, F., Laurion, I., Séjourné, A., Marlin, C., Hatté, C., Costard, F., Fedorov, A., Desyatkin, A., 2021. Seasonal patterns in greenhouse gas emissions from thermokarst lakes in Central Yakutia (Eastern Siberia). Limnol. Oceanogr. 66, S98–S116. https://doi.org/10.1002/lno.11665

Inagaki, T.M., Possinger, A.R., Grant, K.E., Schweizer, S.A., Mueller, C.W., Derry, L.A., Lehmann, J., Kögel-Knabner, I., 2020. Subsoil organo-mineral associations under contrasting climate conditions. Geochim. Cosmochim. Acta 270, 244–263. https://doi.org/10.1016/j.gca.2019.11.030

International Centre for Diffraction Data, 2013. Be confident with pdf2. http://www.icdd.com/products/technicalbulletins/PDF-2_Technical_%20Bulletin.pdf (accessed 5 August 2015).

IPCC, 2021. Summary for Policymakers. In: Climate Change 2021: The Physical Science Basis. Contribution of Working Group I to the Sixth Assessment Report of the Intergovernmental Panel on Climate Change [Masson-Delmotte, V., P. Zhai, A. Pirani, S. L. Connors, C. Péan, S. Berger, N. Caud, Y. Chen, L. Goldfarb, M. I. Gomis, M. Huang, K. Leitzell, E. Lonnoy, J.B.R. Matthews, T. K. Maycock, T. Waterfield, O. Yelekçi, R. Yu and B. Zhou (eds.)]. Cambridge University Press. In Press.

Jakobsen, B.H., Siegert, C., Ostroumov, V., 1996. Effect of permafrost and palaeo-environmental history on soil formation in the lower Kolyma Lowland, Siberia. Dan. J Geogr 96, 40–50.

Johnson, K., Purvis, G., Lopez-Capel, E., Peacock, C., Gray, N., Wagner, T., März, C., Bowen, L., Ojeda, J., Finlay, N., Robertson, S., Worrall, F., Greenwell, C., 2015. Towards a mechanistic understanding of carbon stabilization in manganese oxides. Nat. Commun. 6, 7628. https://doi.org/10.1038/ncomms8628

Jones, B.M., Grosse, G., Farquharson, L.M., Roy-Léveillée, P., Veremeeva, A., Kanevskiy, M.Z., Gaglioti, B.V., Breen, A.L., Parsekian, A.D., Ulrich, M., Hinkel, K.M., 2022. Lake and drained lake basin systems in lowland permafrost regions. Nat. Rev. Earth Environ. 3, 85–98. https://doi.org/10.1038/s43017-021-00238-9

Jongejans, L.L., Liebner, S., Knoblauch, C., Mangelsdorf, K., Strauss, J., 2021a. Cumulative greenhouse gas production in thawed sediments underneath a Yedoma and Alas thermokarst lake in Eastern Siberia. https://doi.org/10.1594/PANGAEA.928140

Jongejans, L.L., Liebner, S., Knoblauch, C., Mangelsdorf, K., Ulrich, M., Grosse, G., Tanski, G., Fedorov, A.N., Konstantinov, P.Y., Windirsch, T., Wiedmann, J., Strauss, J., 2021b. Greenhouse gas production and lipid biomarker distribution in Yedoma and Alas thermokarst lake sediments in Eastern Siberia. Glob. Change Biol. 27, 2822–2839. https://doi.org/10.1111/gcb.15566

Joss, H., Patzner, M.S., Maisch, M., Mueller, C.W., Kappler, A., Bryce, C., 2022. Cryoturbation impacts iron-organic carbon associations along a permafrost soil chronosequence in northern Alaska. Geoderma 413, 115738. https://doi.org/10.1016/j.geoderma.2022.115738

Kappler, A., Bryce, C., Mansor, M., Lueder, U., Byrne, J.M., Swanner, E.D., 2021. An evolving view on biogeochemical cycling of iron. Nat. Rev. Microbiol. https://doi.org/10.1038/s41579-020-00502-7

Kleber, M., Bourg, I.C., Coward, E.K., Hansel, C.M., Myneni, S.C.B., Nunan, N., 2021. Dynamic interactions at the mineral–organic matter interface. Nat. Rev. Earth Environ. https://doi.org/10.1038/s43017-021-00162-y

Kleber, M., Eusterhues, K., Keiluweit, M., Mikutta, C., Mikutta, R., Nico, P.S., 2015. Mineral–Organic Associations: Formation, Properties, and Relevance in Soil Environments, in: Advances in Agronomy. Elsevier, pp. 1–140. https://doi.org/10.1016/bs.agron.2014.10.005

Kleber, M., Sollins, P., Sutton, R., 2007. A conceptual model of organo-mineral interactions in soils: self-assembly of organic molecular fragments into zonal structures on mineral surfaces. Biogeochemistry 85, 9–24. https://doi.org/10.1007/s10533-007-9103-5

Kögel-Knabner, I., Amelung, W., Cao, Z., Fiedler, S., Frenzel, P., Jahn, R., Kalbitz, K., Kölbl, A., Schloter, M., 2010. Biogeochemistry of paddy soils. Geoderma 157, 1–14. https://doi.org/10.1016/j.geoderma.2010.03.009

Kögel-Knabner, I., Guggenberger, G., Kleber, M., Kandeler, E., Kalbitz, K., Scheu, S., Eusterhues, K., Leinweber, P., 2008. Organo-mineral associations in temperate soils: Integrating biology, mineralogy, and organic matter chemistry. J. Plant Nutr. Soil Sci. 171, 61–82. https://doi.org/10.1002/jpln.200700048

Koven, C.D., Ringeval, B., Friedlingstein, P., Ciais, P., Cadule, P., Khvorostyanov, D., Krinner, G., Tarnocai, C., 2011. Permafrost carbon-climate feedbacks accelerate global warming. Proc. Natl. Acad. Sci. 108, 14769–14774. https://doi.org/10.1073/pnas.1103910108

Kramer, M.G., Chadwick, O.A., 2018. Climate-driven thresholds in reactive mineral retention of soil carbon at the global scale. Nat. Clim. Change 8, 1104–1108. https://doi.org/10.1038/s41558-018-0341-4

Lalonde, K., Mucci, A., Ouellet, A., Gélinas, Y., 2012. Preservation of organic matter in sediments promoted by iron. Nature 483, 198–200. https://doi.org/10.1038/nature10855

Li, H., Santos, F., Butler, K., Herndon, E., 2021. A Critical Review on the Multiple Roles of Manganese in Stabilizing and Destabilizing Soil Organic Matter. Environ. Sci. Technol. 55, 12136–12152. https://doi.org/10.1021/acs.est.1c00299

Lim, A.G., Loiko, S.V., Kuzmina, D.M., Krickov, I.V., Shirokova, L.S., Kulizhsky, S.P., Pokrovsky, O.S., 2022a. Organic carbon, and major and trace elements reside in labile low-molecular form in the ground ice of permafrost peatlands: a case study of colloids in peat ice of Western Siberia. Environ. Sci. Process. Impacts. https://doi.org/10.1039/D1EM00547B

Lim, A.G., Loiko, S.V., Pokrovsky, O.S., 2022b. Sizable pool of labile organic carbon in peat and mineral soils of permafrost peatlands, western Siberia. Geoderma 409, 115601. https://doi.org/10.1016/j.geoderma.2021.115601

Lipson, D.A., Zona, D., Raab, T.K., Bozzolo, F., Mauritz, M., Oechel, W.C., 2012. Water-table height and microtopography control biogeochemical cycling in an Arctic coastal tundra ecosystem. Biogeosciences 9, 577–591. https://doi.org/10.5194/bg-9-577-2012

Mehra, O.P., Jackson, M.L., 1960. Iron oxide removal from soils and clays by a dithionite-citrate system buffered with sodium bicarbonate. Clays Clay Miner. 317–327. https://doi.org/10.1016/B978-0-08-009235-5.50026-7

Melton, E.D., Swanner, E.D., Behrens, S., Schmidt, C., Kappler, A., 2014. The interplay of microbially mediated and abiotic reactions in the biogeochemical Fe cycle. Nat. Rev. Microbiol. 12, 797–808. https://doi.org/10.1038/nrmicro3347

Mikutta, C., Wiederhold, J.G., Cirpka, O.A., Hofstetter, T.B., Bourdon, B., Gunten, U.V., 2009. Iron isotope fractionation and atom exchange during sorption of ferrous iron to mineral surfaces. Geochim. Cosmochim. Acta 73, 1795–1812. https://doi.org/10.1016/j.gca.2009.01.014

Mikutta, R., Kleber, M., Torn, M.S., Jahn, R., 2006. Stabilization of Soil Organic Matter: Association with Minerals or Chemical Recalcitrance? Biogeochemistry 77, 25–56. https://doi.org/10.1007/s10533-005-0712-6

Mikutta, R., Mikutta, C., Kalbitz, K., Scheel, T., Kaiser, K., Jahn, R., 2007. Biodegradation of forest floor organic matter bound to minerals via different binding mechanisms. Geochim. Cosmochim. Acta 71, 2569–2590. https://doi.org/10.1016/j.gca.2007.03.002

Miller, K., Lai, C.-T., Dahlgren, R., Lipson, D., 2019. Anaerobic Methane Oxidation in High-Arctic Alaskan Peatlands as a Significant Control on Net CH4 Fluxes. Soil Syst. 3, 7. https://doi.org/10.3390/soilsystems3010007

Miller, K.E., Lai, C.-T., Friedman, E.S., Angenent, L.T., Lipson, D.A., 2015. Methane suppression by iron and humic acids in soils of the Arctic Coastal Plain. Soil Biol. Biochem. 83, 176–183. https://doi.org/10.1016/j.soilbio.2015.01.022

Monhonval, A., Mauclet, E., Pereira, B., Vandeuren, A., Strauss, J., Grosse, G., Schirrmeister, L., Fuchs, M., Kuhry, P., Opfergelt, S., 2021a. Mineral Element Stocks in the Yedoma Domain: A Novel

Method Applied to Ice-Rich Permafrost Regions. Front. Earth Sci. 9, 773. https://doi.org/10.3389/feart.2021.703304

Monhonval, A., Opfergelt, S., Mauclet, E., Pereira, B., Vandeuren, A., Grosse, G., Schirrmeister, L., Fuchs, M., Kuhry, P., Strauss, J., 2020. Yedoma domain Mineral Concentrations Assessment (YMCA). https://doi.org/10.1594/PANGAEA.922724

Monhonval, A., Strauss, J., Mauclet, E., Hirst, C., Bemelmans, N., Grosse, G., Schirrmeister, L., Fuchs, M., Opfergelt, S., 2021b. Iron Redistribution Upon Thermokarst Processes in the Yedoma Domain. Front. Earth Sci. 9, 629. https://doi.org/10.3389/feart.2021.703339

Mu, C.C., Zhang, T.J., Zhao, Q., Guo, H., Zhong, W., Su, H., Wu, Q.B., 2016. Soil organic carbon stabilization by iron in permafrost regions of the Qinghai-Tibet Plateau. Geophys. Res. Lett. 43, 10,286-10,294. https://doi.org/10.1002/2016GL070071

Nierop, K.G.J.J., Jansen, B., Verstraten, J.M., 2002. Dissolved organic matter, aluminium and iron interactions: precipitation induced by metal/carbon ratio, pH and competition. Sci. Total Environ. 300, 201–211. https://doi.org/10.1016/S0048-9697(02)00254-1

Oades, J.M., 1988. The retention of organic matter in soils. Biogeochemistry 5, 35–70. https://doi.org/10.1007/BF02180317

Oldham, V.E., Mucci, A., Tebo, B.M., Luther, G.W., 2017. Soluble Mn(III)–L complexes are abundant in oxygenated waters and stabilized by humic ligands. Geochim. Cosmochim. Acta 199, 238–246. https://doi.org/10.1016/j.gca.2016.11.043

Opfergelt, S., 2020. The next generation of climate model should account for the evolution of mineral-organic interactions with permafrost thaw. Environ. Res. Lett. 15, 091003. https://doi.org/10.1088/1748-9326/ab9a6d

Page, A.L., Miller, R.H., Keeney, D.R., 1982. Methods of soil analysis; part 2. Chemical and Microbiological Properties. Am. Soc Agron. Publ 363–364.

Pan, Y., Koopmans, G.F., Bonten, L.T.C., Song, J., Luo, Y., Temminghoff, E.J.M., Comans, R.N.J., 2014. Influence of pH on the redox chemistry of metal (hydr)oxides and organic matter in paddy soils. J. Soils Sediments 14, 1713–1726. https://doi.org/10.1007/s11368-014-0919-z

Patrick Jr., W.H., Jugsujinda, A., 1992. Sequential Reduction and Oxidation of Inorganic Nitrogen, Manganese, and Iron in Flooded Soil. Soil Sci. Soc. Am. J. 56, 1071–1073. https://doi.org/10.2136/sssaj1992.03615995005600040011x

Patzner, M.S., Mueller, C.W., Malusova, M., Baur, M., Nikeleit, V., Scholten, T., Hoeschen, C., Byrne, J.M., Borch, T., Kappler, A., Bryce, C., 2020. Iron mineral dissolution releases iron and associated organic carbon during permafrost thaw. Nat. Commun. 11, 6329. https://doi.org/10.1038/s41467-020-20102-6

Pestryakova, L.A., Herzschuh, U., Wetterich, S., Ulrich, M., 2012. Present-day variability and Holocene dynamics of permafrost-affected lakes in central Yakutia (Eastern Siberia) inferred from diatom records. Quat. Sci. Rev. 51, 56–70. https://doi.org/10.1016/j.quascirev.2012.06.020

Possinger, A.R., Bailey, S.W., Inagaki, T.M., Kögel-Knabner, I., Dynes, J.J., Arthur, Z.A., Lehmann, J., 2020. Organo-mineral interactions and soil carbon mineralizability with variable saturation cycle frequency. Geoderma 375, 114483. https://doi.org/10.1016/j.geoderma.2020.114483

R Core Team, 2018. R: A language and environment for statistical computing. R Foundation for Statistical Computing, Vienna, Austria. URL https://www.R-project.org/.

Ravansari, R., Wilson, S.C., Tighe, M., 2020. Portable X-ray fluorescence for environmental assessment of soils: Not just a point and shoot method. Environ. Int. 134, 105250. https://doi.org/10.1016/j.envint.2019.105250

Regelink, I.C., Voegelin, A., Weng, L., Koopmans, G.F., Comans, R.N.J., 2014. Characterization of Colloidal Fe from Soils Using Field-Flow Fractionation and Fe K-Edge X-ray Absorption Spectroscopy. Environ. Sci. Technol. 48, 4307–4316. https://doi.org/10.1021/es405330x

Rennert, T., 2019. Wet-chemical extractions to characterise pedogenic Al and Fe species – a critical review. Soil Res. 57, 1. https://doi.org/10.1071/SR18299

Rowley, M.C., Grand, S., Verrecchia, É.P., 2018. Calcium-mediated stabilisation of soil organic carbon. Biogeochemistry 137, 27–49. https://doi.org/10.1007/s10533-017-0410-1

Schirrmeister, L., Dietze, E., Matthes, H., Grosse, G., Strauss, J., Laboor, S., Ulrich, M., Kienast, F., Wetterich, S., 2020. The genesis of Yedoma Ice Complex permafrost - grain-size endmember

modeling analysis from Siberia and Alaska. EampG Quat. Sci. J. 69, 33–53. https://doi.org/10.5194/egqsj-69-33-2020

Schirrmeister, L., Froese, D., Tumskoy, V., Grosse, G., Wetterich, S., 2013. Yedoma: Late Pleistocene ice-rich syngenetic permafrost of Beringia, in: Encyclopedia of Quaternary Science. 2nd Edition. Elsevier, pp. 542–552.

Schirrmeister, L., Wetterich, S., Schwamborn, G., Matthes, H., Grosse, G., Klimova, I., Kunitsky, V.V., Siegert, C., 2022. Heavy and Light Mineral Association of Late Quaternary Permafrost Deposits in Northeastern Siberia. Front. Earth Sci. 10. https://doi.org/10.3389/feart.2022.741932

Schmidt, M.W.I., Torn, M.S., Abiven, S., Dittmar, T., Guggenberger, G., Janssens, I.A., Kleber, M., Kögel-Knabner, I., Lehmann, J., Manning, D.A.C., Nannipieri, P., Rasse, D.P., Weiner, S., Trumbore, S.E., 2011. Persistence of soil organic matter as an ecosystem property. Nature 478, 49–56. https://doi.org/10.1038/nature10386

Schneider von Deimling, T., Grosse, G., Strauss, J., Schirrmeister, L., Morgenstern, A., Schaphoff, S., Meinshausen, M., Boike, J., 2015. Observation-based modelling of permafrost carbon fluxes with accounting for deep carbon deposits and thermokarst activity. Biogeosciences 12, 3469–3488. https://doi.org/10.5194/bg-12-3469-2015

Schuur, E.A.G., McGuire, A.D., Schädel, C., Grosse, G., Harden, J.W., Hayes, D.J., Hugelius, G., Koven, C.D., Kuhry, P., Lawrence, D.M., Natali, S.M., Olefeldt, D., Romanovsky, V.E., Schaefer, K., Turetsky, M.R., Treat, C.C., Vonk, J.E., 2015. Climate change and the permafrost carbon feedback. Nature 520, 171–179. https://doi.org/10.1038/nature14338

Schwertmann, U., 1991. Solubility and dissolution of iron oxides. Plant Soil 130, 1–25. https://doi.org/10.1007/BF00011851

Schwesig, D., Kalbitz, K., Matzner, E., 2003. Effects of aluminium on the mineralization of dissolved organic carbon derived from forest floors. Eur. J. Soil Sci. 54, 311–322. https://doi.org/10.1046/j.1365-2389.2003.00523.x

Soloviev, P.A., 1959. Cryolithic Zone of the Northern Part of Lena-Amga Interfluve. Izd. Akad. SSSR 142.

Sowers, T.D., Wani, R.P., Coward, E.K., Fischel, M.H.H., Betts, A.R., Douglas, T.A., Duckworth, O.W., Sparks, D.L., 2020. Spatially Resolved Organomineral Interactions across a Permafrost Chronosequence. Environ. Sci. Technol. acs.est.9b06558. https://doi.org/10.1021/acs.est.9b06558

Stevenson, F.J., 1994. Humus chemistry: genesis, composition, reactions. John Wiley & Sons.

Strauss, J., Laboor, S., Schirrmeister, L., Fedorov, A.N., Fortier, D., Froese, D., Fuchs, M., Günther, F., Grigoriev, M., Harden, J., Hugelius, G., Jongejans, L.L., Kanevskiy, M., Kholodov, A., Kunitsky, V., Kraev, G., Lozhkin, A., Rivkina, E., Shur, Y., Siegert, C., Spektor, V., Streletskaya, I., Ulrich, M., Vartanyan, S., Veremeeva, A., Anthony, K.W., Wetterich, S., Zimov, N., Grosse, G., 2021. Circum-Arctic Map of the Yedoma Permafrost Domain. Front. Earth Sci. 9. https://doi.org/10.3389/feart.2021.758360

Strauss, J., Schirrmeister, L., Grosse, G., Fortier, D., Hugelius, G., Knoblauch, C., Romanovsky, V., Schädel, C., Schneider von Deimling, T., Schuur, E.A.G., Shmelev, D., Ulrich, M., Veremeeva, A., 2017. Deep Yedoma permafrost: A synthesis of depositional characteristics and carbon vulnerability. Earth-Sci. Rev. 172, 75–86. https://doi.org/10.1016/j.earscirev.2017.07.007

Tarasenko, T.V., 2013. Interannual variations in the areas of thermokarst lakes in Central Yakutia. Water Resour. 40, 111–119. https://doi.org/10.1134/S0097807813010107

Torn, M.S., Trumbore, S.E., Chadwick, O.A., Vitousek, P.M., Hendricks, D.M., 1997. Mineral control of soil organic carbon storage and turnover. Nature 389, 170–173. https://doi.org/10.1038/38260

Ulrich, M., Jongejans, L.L., Grosse, G., Schneider, B., Opel, T., Wetterich, S., Fedorov, A.N., Schirrmeister, L., Windirsch, T., Wiedmann, J., Strauss, J., 2021. Geochemistry and Weathering Indices of Yedoma and Alas Deposits beneath Thermokarst Lakes in Central Yakutia. Front. Earth Sci. 9, 701. https://doi.org/10.3389/feart.2021.704141

Ulrich, M., Matthes, H., Schirrmeister, L., Schütze, J., Park, H., Iijima, Y., Fedorov, A.N., 2017. Differences in behavior and distribution of permafrost-related lakes in Central Yakutia and their response to climatic drivers. Water Resour. Res. 53, 1167–1188. https://doi.org/10.1002/2016WR019267

Ulrich, M., Matthes, H., Schmidt, J., Fedorov, A.N., Schirrmeister, L., Siegert, C., Schneider, B., Strauss, J., Zielhofer, C., 2019. Holocene thermokarst dynamics in Central Yakutia – A multi-core and robust grain-size endmember modeling approach. Quat. Sci. Rev. 218, 10–33. https://doi.org/10.1016/j.quascirev.2019.06.010

von Lützow, M., Kogel-Knabner, I., Ekschmitt, K., Matzner, E., Guggenberger, G., Marschner, B., Flessa, H., 2006. Stabilization of organic matter in temperate soils: mechanisms and their relevance under different soil conditions - a review. Eur. J. Soil Sci. 57, 426–445. https://doi.org/10.1111/j.1365-2389.2006.00809.x

Wagai, R., Mayer, L.M., 2007. Sorptive stabilization of organic matter in soils by hydrous iron oxides. Geochim. Cosmochim. Acta 71, 25–35. https://doi.org/10.1016/j.gca.2006.08.047

Wagai, R., Mayer, L.M., Kitayama, K., Shirato, Y., 2013. Association of organic matter with iron and aluminum across a range of soils determined via selective dissolution techniques coupled with dissolved nitrogen analysis. Biogeochemistry 112, 95–109. https://doi.org/10.1007/s10533-011-9652-5

Wang, S., Jia, Y., Liu, T., Wang, Y., Liu, Z., Feng, X., 2021. Delineating the Role of Calcium in the Large-Scale Distribution of Metal-Bound Organic Carbon in Soils. Geophys. Res. Lett. 48, e2021GL092391. https://doi.org/10.1029/2021GL092391

Wang, X., Toner, B.M., Yoo, K., 2019. Mineral vs. organic matter supply as a limiting factor for the formation of mineral-associated organic matter in forest and agricultural soils. Sci. Total Environ. 692, 344–353. https://doi.org/10.1016/j.scitotenv.2019.07.219

Windirsch, T., Grosse, G., Ulrich, M., Schirrmeister, L., Fedorov, A.N., Konstantinov, P.Y., Fuchs, M., Jongejans, L.L., Wolter, J., Opel, T., Strauss, J., 2020. Organic carbon characteristics in ice-rich permafrost in alas and Yedoma deposits, central Yakutia, Siberia. Biogeosciences 17, 3797–3814. https://doi.org/10.5194/bg-17-3797-2020

Winkler, P., Kaiser, K., Thompson, A., Kalbitz, K., Fiedler, S., Jahn, R., 2018. Contrasting evolution of iron phase composition in soils exposed to redox fluctuations. Geochim. Cosmochim. Acta 235, 89–102. https://doi.org/10.1016/j.gca.2018.05.019

Xue, B., Huang, L., Huang, Y., Zhou, F., Li, F., Kubar, K.A., Li, X., Lu, J., Zhu, J., 2019. Roles of soil organic carbon and iron oxides on aggregate formation and stability in two paddy soils. Soil Tillage Res. 187, 161–171. https://doi.org/10.1016/j.still.2018.12.010

Zhao, Q., Adhikari, D., Huang, R., Patel, A., Wang, X., Tang, Y., Obrist, D., Roden, E.E., Yang, Y., 2017. Coupled dynamics of iron and iron-bound organic carbon in forest soils during anaerobic reduction. Chem. Geol. 464, 118–126. https://doi.org/10.1016/j.chemgeo.2016.12.014